Observation of Quasi-2-Day Convective Disturbances in the Equatorial Indian Ocean during DYNAMO

HUNGJUI YU

Department of Atmospheric Sciences, National Taiwan University, Taipei, Taiwan

RICHARD H. JOHNSON AND PAUL E. CIESIELSKI

Department of Atmospheric Science, Colorado State University, Fort Collins, Colorado

HUNG-CHI KUO

Department of Atmospheric Sciences, National Taiwan University, Taipei, Taiwan

(Manuscript received 22 November 2017, in final form 22 May 2018)

ABSTRACT

This study examines the westward-propagating convective disturbances with quasi-2-day intervals of occurrence identified over Gan Island in the central Indian Ocean from mid- to late October 2011 during the Dynamics of the Madden–Julian Oscillation (DYNAMO) field campaign. Atmospheric sounding, satellite, and radar data are used to develop a composite of seven such disturbances. Composites and spectral analyses reveal that 1) the quasi-2-day convective events comprise westward-propagating diurnal convective disturbances with phase speeds of 10–12 m s^{-1} whose amplitudes are modulated on a quasi-2-day time scale on a zonal scale of ~1000 km near the longitudes of Gan; 2) the cloud life cycle of quasi-2-day convective disturbances shows a distinct pattern of tropical cloud population evolution—from shallow to deep to stratiform convection; 3) the time scales of mesoscale convective system development and boundary layer modulation play essential roles in determining the periodicity of the quasi-2-day convective events; and 4) in some of the quasi-2-day events there is evidence of counterpropagating (westward and eastward) cloud systems along the lines proposed by Yamada et al. Based on these findings, an interpretation is proposed for the mechanisms for the quasi-2-day disturbances observed during DYNAMO that combines concepts from prior studies of this phenomenon over the western Pacific and Indian Oceans.

1. Introduction

Convectively active, westward-propagating disturbances with a quasi-2-day periodicity are frequently associated with intraseasonal oscillations (ISOs) over the tropical western Pacific (WPAC; Nakazawa 1988, 1995; Lau et al. 1991; Hendon and Liebmann 1994; Takayabu 1994a,b; Takayabu et al. 1996; Chen et al. 1996). In particular, these convective disturbances received considerable attention in studies based on observations taken during the Tropical Ocean and Global Atmosphere Coupled Ocean–Atmosphere Response Experiment (TOGA COARE) intensive observation period (IOP) in 1992–93 over the equatorial WPAC (Takayabu 1994a,b; Takayabu et al. 1996; Chen et al. 1996; Haertel and Johnson 1998; Haertel and Kiladis 2004). These studies regarded the 2-day convective events as convectively coupled equatorial waves, referred to as "2-day waves," characterized by zonal wavelengths of 2000–4000 km and westward propagation of 10–15 m s^{-1} (Hendon and Liebmann 1994; Takayabu 1994b; Takayabu et al. 1996; Chen et al. 1996; Haertel and Johnson 1998; Wheeler et al. 2000) and associated with the $n = 1$ inertio-gravity wave (IGW) with equivalent depths of 12–50 m (Takayabu 1994a; Wheeler and Kiladis 1999). Observations from TOGA COARE also revealed that the quasi-2-day waves were composed of westward-propagating organized cloud clusters (Chen et al. 1996; Chen and Houze 1997) and further indicated that the quasi-2-day convective disturbances possessed a life cycle similar to that of organized mesoscale convective systems (MCSs) or long-lived squall lines, with a transition from predominantly shallow to deep to

Corresponding author: Hung-Chi Kuo, kuo@as.ntu.edu.tw

DOI: 10.1175/JAS-D-17-0351.1

stratiform convection (Hendon and Liebmann 1994; Takayabu et al. 1996), which repeated at quasi-2-day intervals from local observations.

To explain the quasi-2-day intervals of occurrence, Chen and Houze (1997) suggested that the near-2-day periodicity results from an interaction between the 2-day waves and convection. A conceptual mesoscale process was proposed involving the nonlinear interaction between clouds, radiation, and surface processes, the so-called ''diurnal dancing'' of convective systems, to explain the near 2-day periodicity. In their scenario, despite diurnal radiative forcing, boundary layer (BL) recovery extends to a second day, likely due to the expanded stratiform clouds of MCSs, which impacts the timing of the next round of convection. The BL recovery for a future convective event over a given region is delayed for up to 12–18 h by the previous convective systems.

Leveraging both satellite IR and microwave data along with ground-based radar observations during the *Mirai* Indian Ocean (IO) cruise for the Study of the Madden–Julian Oscillation Convective Onset (MISMO) experiment (Yoneyama et al. 2008) conducted in the boreal fall of 2006, Yamada et al. (2010) detected a complicated relationship between eastward-propagating precipitating systems and westward-moving upper-level cloud shields. The eastward-propagating systems, generally less than 10 km in depth, deepened when they encountered the moisture-rich environment of the westward-moving, upper-level stratiform clouds yielding a 2–4 day periodicity in rainfall at a given longitude. These stratiform cloud shields, advected by upper-level easterly flow, were trailing clouds remnants from previous eastward-propagating convective systems.

In addition to these quasi-2-day features observed in previous field campaigns, westward-propagating mesoscale convective events with a similar periodicity were also prominent over the equatorial IO within the convective envelope of the October Madden–Julian oscillation (MJO) event during the Dynamics of the Madden–Julian Oscillation (DYNAMO)/Atmospheric Radiation Measurement MJO Investigation Experiment (AMIE)/Cooperative Indian Ocean Experiment on Intraseasonal Variability in the Year 2011 (CINDY) field campaign (Johnson and Ciesielski 2013; Yoneyama et al. 2013; Zuluaga and Houze 2013; Johnson et al. 2015). The field campaign (hereafter DYNAMO) was designed to observe and understand the initiation of the MJO over the IO. Its observational network consisted of a large suite of measurements of the atmosphere and ocean, but for this study, high-resolution upper-air radiosonde data and remote sensor retrievals from radars and satellites are utilized. Seven quasi-2-day convective events with significant rainfall identified in the last half of October by data from Gan Island in the central IO are used to form a composite view of the wind, thermodynamic, and diabatic structure of the disturbances. These events were included in a prior study by Zuluaga and Houze (2013), although their composite analysis also includes events on a 4–6-day time scale associated with synoptic-scale waves from the November MJO.

The observational datasets and the analysis procedures used in the study are described in section 2. The methodology for identifying the quasi-2-day convective events is explained in section 3. Large-scale convective features of these events, including their propagation and the spatial scale, are shown in section 4. In section 5, differences between the quasi-2-day and diurnal convection are discussed. The composite atmospheric structures and life cycle of the quasi-2-day convective disturbances are analyzed in section 6. In section 7, an interpretation of the quasi-2-day convective disturbances is proposed. Finally, section 8 summarizes the observational results.

2. Data and analysis procedures

This study utilizes data from various observational platforms employed during the DYNAMO special observing period (SOP; 1 October–28 November 2011), in particular, data from the Gan Island site located on Addu Atoll (hereafter, Gan) at 0.69°S, 73.15°E. Seven quasi-2-day convective disturbances were observed from 15 to 31 October 2011 to pass the Gan location. Datasets used in this study are listed below.

a. Gridded satellite data

The 5-km-resolution, 3-hourly-interpolated *Meteosat-7* infrared (channel 8) brightness temperature (IRBT) data (UCAR/NCAR 2012) and the 0.25° resolution, 3-hourly rain-rate estimates from Tropical Rainfall Measuring Mission (TRMM) 3B42V7 dataset (TRMM 2011) are both employed in this study. The major purpose of these datasets is to identify the occurrences of the quasi-2-day convective events as well as their broadscale features.

b. Upper-air radiosonde observations

The DYNAMO enhanced sounding array (ESA) was composed of six sites forming two quadrilateral arrays (northern and southern sounding array) in the central equatorial IO during SOP (Fig. 1). The purpose of these sounding sites was to observe the evolution of atmospheric vertical structures using 3–6-hourly, high-vertical-resolution radiosondes and to compute the large-scale forcing fields as well as heat and moisture budgets (Johnson and Ciesielski 2013; Yoneyama et al. 2013; Johnson et al. 2015). This study uses primarily the 3-hourly sounding data from Gan during the DYNAMO

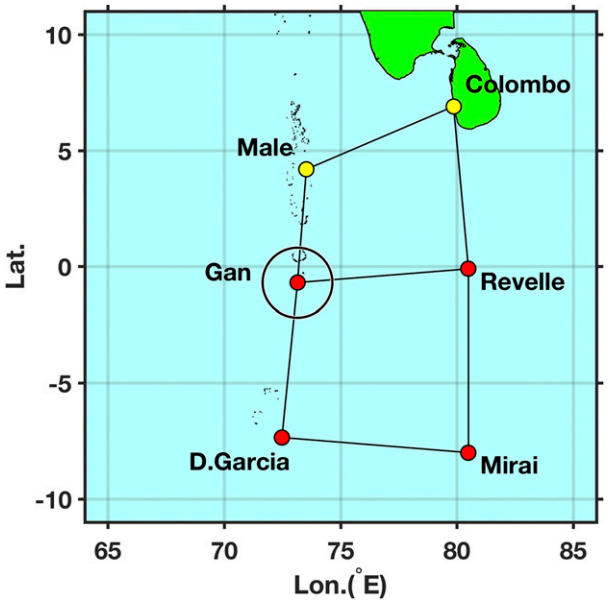

FIG. 1. The DYNAMO ESA in the central equatorial IO during DYNAMO SOP. High-frequency sounding sites with eight launches (four launches) per day are indicated with red (yellow) circles. Most analyses in this study focus on Gan at 0.69°S, 73.15°E. The outer black circle around Gan indicates the 150-km-radius circular region for satellite data averaging and the AMIE-Gan large-scale objective analysis domain.

SOP. The high-resolution sounding data were interpolated to 5 hPa for use in this study. Details of the sounding systems, observing characteristics, and quality-control procedures for DYNAMO soundings are contained in Ciesielski et al. (2014).

c. *AMIE-Gan large-scale objective analysis*

Large-scale fields, including apparent heating Q_1, apparent drying Q_2, and large-scale vertical motion, were obtained from AMIE-Gan objective analyses patterned after the procedure of Xie et al. (2004). These analyses, covering a nearly circular region with 150-km radius centered on Gan (as illustrated in Fig. 1), were available from 2 October to 31 December 2011 at 3-h temporal resolution. The dataset was constructed by using the variational analysis method described in Zhang and Lin (1997) and Zhang et al. (2001) and was constrained by C-band Shared Mobile Atmospheric Research and Teaching Radar (SMART-R) rainfall estimates $P_{\text{SMART-R}}$ adjusted with TRMM rainfall P_{TRMM} using a procedure described in Ciesielski et al. (2017). This adjustment retains the variability of the TRMM 3B42 rainfall but with the magnitude set by the SMART-R. Use of the surface rainfall constraint in the analyses ensures that the vertically integrated large-scale heat and moisture budgets are consistent with the observed precipitation over the region.

d. *CombRet dataset*

Vertical profiles of the shortwave (SW) and longwave (LW) radiative fluxes and heating rates were obtained from the Pacific Northwest National Laboratory (PNNL) Combined Retrieval (CombRet) dataset (Feng et al. 2014). The CombRet radar product includes high-resolution data from the SMART-R, NCAR's S-band dual-polarization Doppler radar (S-Pol), and the Ka-band ARM zenith radar (KAZR) deployed on Gan. The radiative product was retrieved by using a delta-four-stream correlated-k distribution radiative transfer model (Mather et al. 2007, Fu and Liou 1992). CombRet is available at 1-h, 25-hPa resolution (from 1000 to 50 hPa) for the period from 10 October 2011 to 8 February 2012. It was averaged into 3-h bins to match the temporal resolution of the satellite, rainfall, and sounding data. The version of CombRet data used in this study was produced by replacing the observed 2-m temperature with the SST in the near vicinity of Gan, which makes the radiative fields more representative of open-ocean conditions. Radiative fields are available for both all-sky and clear-sky conditions, allowing us to estimate cloud radiative forcing effects.

e. *Computation of vertical flux of moist static energy*

The vertical eddy flux of MSE (F_{MSE}) has been widely used to measure the activity of cumulus convection (Yanai et al. 1973; Gallus and Johnson 1991; Johnson et al. 2015). In this study, the composite F_{MSE} is estimated following Yanai et al. (1973):

$$F_{\text{MSE}} = \frac{1}{g}\int_{P_{100\text{hPa}}}^{P} (Q_1 - Q_2 - Q_R)\, dp \cong -\frac{1}{g}\overline{h'\omega'},$$

in which F_{MSE} indicates the vertical eddy flux of MSE (h) and Q_1 and Q_2 were obtained from AMIE-Gan analysis, while Q_R (≡SW + LW) is the net radiative heating rate retrieved from CombRet data. Next, $(Q_1 - Q_2 - Q_R)$ was integrated downward from 100 hPa (a reasonable cloud-top pressure where F_{MSE} equals zero) to each pressure level to estimate the F_{MSE} profiles as $-(1/g)\overline{h'\omega'}$.

3. Identification of the quasi-2-day convective events

This study focuses on the convective activities over the central IO, especially the area around Gan (as illustrated in Fig. 1). During the convectively active period of the October MJO over this region (15–31 October 2011), convective activity and precipitation tended to occur at quasi-2-day intervals (Zuluaga and Houze 2013),

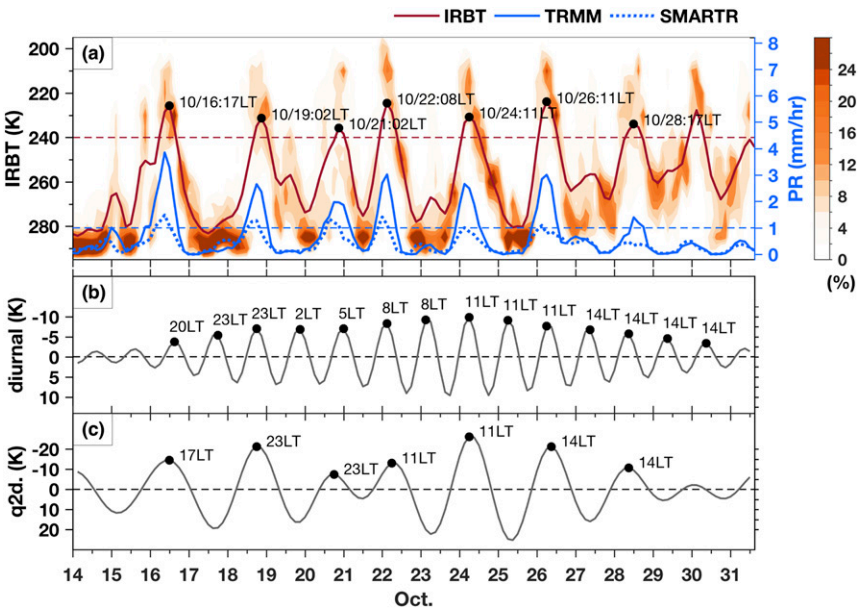

FIG. 2. (a) Time series of IRBT areal percentage in 5-K intervals (%; colored) and 6-hourly running-averaged IRBT (K; red solid curve), TRMM 3B42 rain rate (mm h^{-1}; blue solid curve), and adjusted SMART-R surface rain rate (mm h^{-1}; blue dotted curve) over the 150-km radius circular region around Gan (as indicated in Fig. 1) during late October 2011. The times of seven selected quasi-2-day (q2d) convective events are indicated with black dots and labeled with local time at Gan (UTC + 5 h). The criteria for the convectively active events are indicated with IRBT peaks <240 K (red dashed line) and averaged TRMM rain-rate peaks >1 mm h^{-1} (blue dashed line). (b) Time series of filtered IRBT signal within a diurnal frequency band (0.9–1.2 days). The dashed black line indicates zero. (c) As in (b), but for quasi-2-day frequency band (1.6–3 days). Times of low peaks are indicated in both (b) and (c) with black dots and labeled with local time at Gan (UTC + 5 h). Note that the ordinates for IRBT on the left are in reverse order and the abscissa indicates the date time in UTC (0000 UTC).

as shown in the time series of average and areal percentage of IRBT, averaged TRMM rain rate, and adjusted SMART-R surface rain rate (Fig. 2a). The IRBT areal percentage in Fig. 2a was calculated by dividing the number of IRBT grid points in 5-K intervals by the total number of grid points over the 150-km circular region around Gan.

From the time series, seven convective events are identified with quasi-2-day periodicity and convective activity characterized by clouds with a mean IRBT minimum below 240 K and rain rates higher than 1 mm h^{-1} in TRMM or SMART-R over the 150-km region near Gan. The criteria and times of these events are listed in Table 1 and indicated in Fig. 2a. These times of IRBT minimal peaks were used as the 0 h for the 48-h-window composite analyses in the later sections. The convective event on 30 October showed an averaged IRBT lower than 240 K; however, it was excluded from the composite analyses because the mean rainfall near Gan was considerably less than the other events and the radar reflectivity indicated mostly stratiform clouds over Gan throughout the day (not shown). By way of comparison, the first six of the seven convective events identified by the IRBT and rain-rate signatures in our study were included in the 11-case composite of Zuluaga and Houze (2013) based on hourly S-Pol rain accumulation. Although the sample size in our study is small, there appears to be no preferred time of day for the 0-h occurrence of these events.

4. Large-scale convective features of the quasi-2-day convective events

One of the conspicuous large-scale convective features during DYNAMO SOP was the eastward-moving MJO convective envelope passing over Gan and the DYNAMO ESA from 15 to 31 October 2011. During this convectively active period over the central IO, hereafter referred to as MJO1, seven quasi-2-day convective events occurred at Gan. According to the IRBT areal percentage in Fig. 2a, during MJO1 the

TABLE 1. Date and time of the minimum peaks of 6-hourly averaged IRBT over 150-km radius around Gan. The seven most convectively active events with quasi-2-day intervals of occurrence were selected during 15–31 Oct 2011 in DYNAMO. LT = UTC + 5 h.

Date	Time (UTC)
16 Oct 2011	1200
18 Oct 2011	2100
20 Oct 2011	2100
22 Oct 2011	0300
24 Oct 2011	0600
26 Oct 2011	0600
28 Oct 2011	1200

frequency of shallow cloud tops reached a maximum before the rainfall peaks. The clouds then evolved into a deeper structure and reached maturity when the lowest IRBT peaks occurred. Following the mature stage, deep convective cores gradually dissipated while the frequency of warmer cloud tops (250–270 K), some of which may be stratiform in nature, maximized (Zuluaga and Houze 2013; Zhang and Yoneyama 2017). These convective transitions repeated at quasi-2-day intervals during MJO1. A second major MJO event occurred over the IO in November with a convectively active phase at Gan from 15 to 30 November 2011; however, for reasons that are not well understood, the quasi-2-day convective signal was not statistically significant over the central IO region during this period and therefore is not considered in this study.

Figure 3 is a time–longitude diagram of IRBT and TRMM rain rate averaged over a 1.5° latitude strip north and south of Gan showing the large-scale zonal features of these quasi-2-day convective events. During DYNAMO, the convective envelope of the October MJO initiated over 60°–70°E on 14 October, slowly propagated eastward through the DYNAMO ESA (72°–80°E) during 15–31 October, which then encountered the diurnally excited, westward-propagating convective signal from Sumatra in early November. As observed in many previous studies, although the MJO convective signal over IO propagated eastward, the convective envelope was composed of a number of westward-propagating features with the shorter time scales (Nakazawa 1988, 1995; Hendon and Liebmann 1994; Takayabu 1994a,b; Takayabu et al. 1996; Chen et al. 1996). The diurnally pulsing, westward-moving convection near the west coast of the island of Sumatra (90°–100°E) may have had some linkages to the convection over the central IO (Kubota et al. 2015); however, such a linkage is not entirely obvious from Fig. 3.

Focusing on the quasi-2-day convective events over Gan, Fig. 4 depicts the time–longitude IRBT and

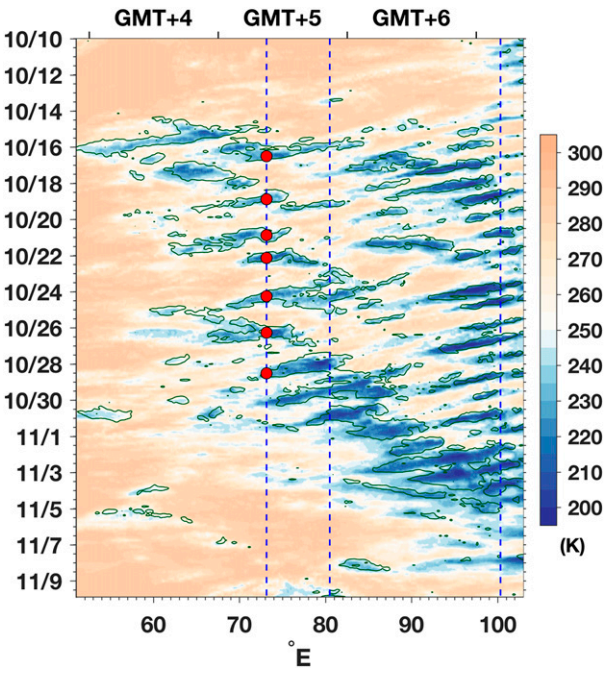

FIG. 3. Time–longitude diagram of IRBT (K; colored) and TRMM rain rate (green contours for 1 mm h^{-1}) averaged over 150 km north and south of the latitude of Gan over the IO region from 10 Oct to 10 Nov 2011. The blue dashed lines, from left to right, indicate the longitudes of sites at Gan Island (73.15°E), R/V *Revelle* (80.5°E), and Padang on Sumatra (100.35°E). The red dots along the longitude of Gan Island indicate the time of convective events listed in Table 1. The ordinate is the date time in UTC (0000 UTC), and the upper abscissa is the local time zone to UTC.

TRMM rain-rate composites of the seven events over the DYNAMO ESA. The reference time (0 h), corresponding to the times listed in Table 1, is characterized by the lowest-averaged IRBT over Gan. In Fig. 4, the region of convective activity propagated westward from the eastern portion of the ESA, peaking over the area surrounding Gan with dominant cold clouds and heavy rainfall near 0 h. The broad zonal scale of the convection (~500–1000 km) suggests the presence of anvil shields and is consistent in size with observations made in TOGA COARE (Takayabu et al. 1996). After time 0 h, the convective signal continued to move westward while the peak IRBT gradually warmed at Gan, suggesting (and confirmed later) that broad areas of stratiform convection dominated during this period.

The westward propagation speed of the convective signals can also be estimated from Fig. 4. Considering time–longitude IRBT composites lower than 240 K, the convective signal propagated 7°–8° in longitude in 20 h, while the rainfall signal showed a similar speed but extended over a greater zonal distance. The propagation speed of the quasi-2-day convective signal is thus

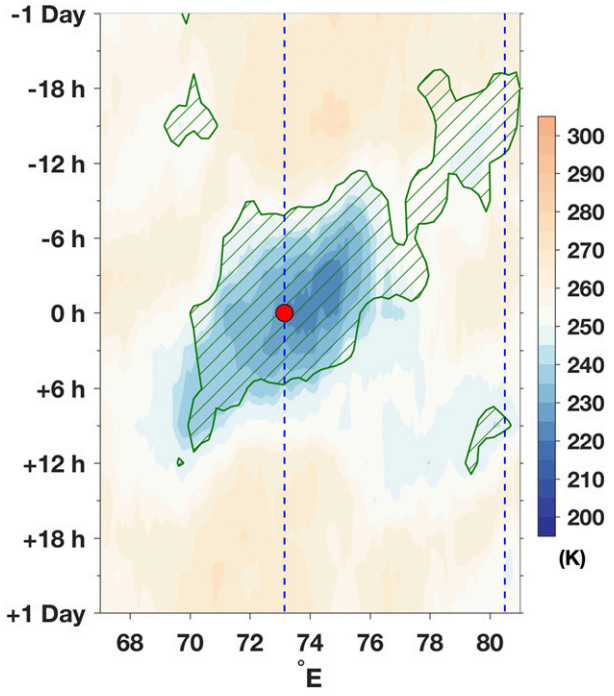

FIG. 4. As in Fig. 3, but for the quasi-2-day convective events composite. The red dot in the center indicates 0 h of each case. The green hatched contours indicate the TRMM rain-rate composite >1 mm h^{-1}, and the blue dashed lines, from left to right, indicate the longitudes of Gan Island and R/V *Revelle*.

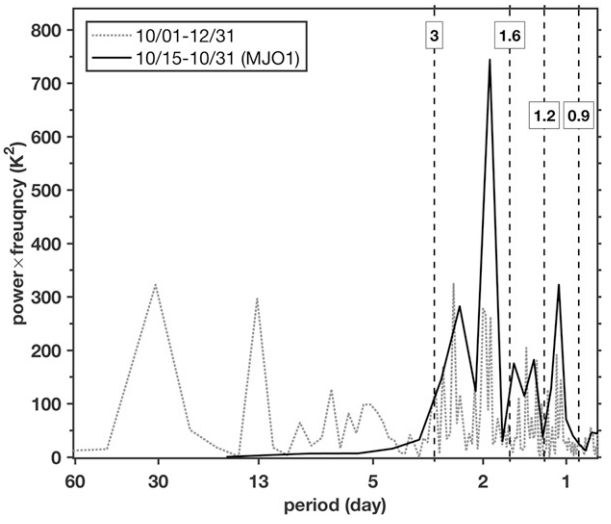

FIG. 5. Fourier power spectrum of averaged IRBT over the 150-km region around Gan during October–December 2011 (gray dotted) and MJO1 period (black solid). The vertical dashed lines from left to right correspond to the periods of 3, 1.6, 1.2, and 0.9 days, as labeled.

approximated to be 10–12 m s^{-1}, the same order as that observed over different areas in previous studies, that is, 10–19 m s^{-1} over WPAC during TOGA COARE IOP in 1992–93 (Haertel and Johnson 1998; Takayabu 1994b) and 15 m s^{-1} in Hendon and Liebmann (1994).

While the quasi-2-day convective events over the equatorial IO possess similar propagation speeds as those over the WPAC, the zonal scales are different. In Figs. 3 and 4, the zonal scale of propagation for the 2-day disturbances is ~1000–1500 km, shorter than the ~2000–4000-km scale observed for the WPAC during the TOGA COARE IOP (Chen et al. 1996; Chen and Houze 1997; Clayson et al. 2002). The difference could well be related to differences in the environments between the two ocean basins, but a full explanation is beyond the scope of this study.

5. Propagating convective waves and stationary convective disturbances

During MJO1, the passage of the westward-propagating quasi-2-day convective events regulated the cloudiness over Gan. To investigate the cloud variability, Fourier spectral analysis is employed to quantify the frequency and intensity of cloud activity associated with the quasi-2-day disturbances during MJO1.

Identical with the procedure in Haertel and Johnson (1998), Fig. 5 shows the Fourier power spectrum of the averaged IRBT over the 150-km region around Gan from October to December 2011 and during MJO1. Here the spectral components are weighted by frequency so that within a certain frequency band, the variance of IRBT time series is proportional to the area under the peak. From October to December, significant spectral peaks are seen at 30, 13, 5, and ~2 days (dotted curve in Fig. 5). These results are similar to the findings in TOGA COARE over WPAC (Haertel and Johnson 1998, their Fig. 5) except for the shorter 30-day oscillation of the ISOs in DYNAMO compared to 60-day in TOGA COARE, due to the MJO events passing over Gan in late 2011 with a time interval of about 30 days (Johnson and Ciesielski 2013; Yoneyama et al. 2013). The peaks in both the diurnal (0.9–1.2 days) and quasi-2-day (1.6–3 days) frequency bands are statistically significant, but the diurnal oscillation was weaker than the quasi-2-day oscillation over this region for both periods. The quasi-2-day (diurnal) cloud oscillation contributed approximately 54.7% (12.3%) of the variance during MJO1 over Gan and about 15.7% (3.2%) from October to December 2011. The quasi-2-day oscillation contributed about 17% of the variance over the Intensive Flux Array in TOGA COARE from November 1992 to February 1993 (Haertel and Johnson 1998).

By applying a Lanczos bandpass filter (Duchon 1979; Thomson and Emery 2014), the diurnal and quasi-2-day oscillations in IRBT during MJO1 can be separated as

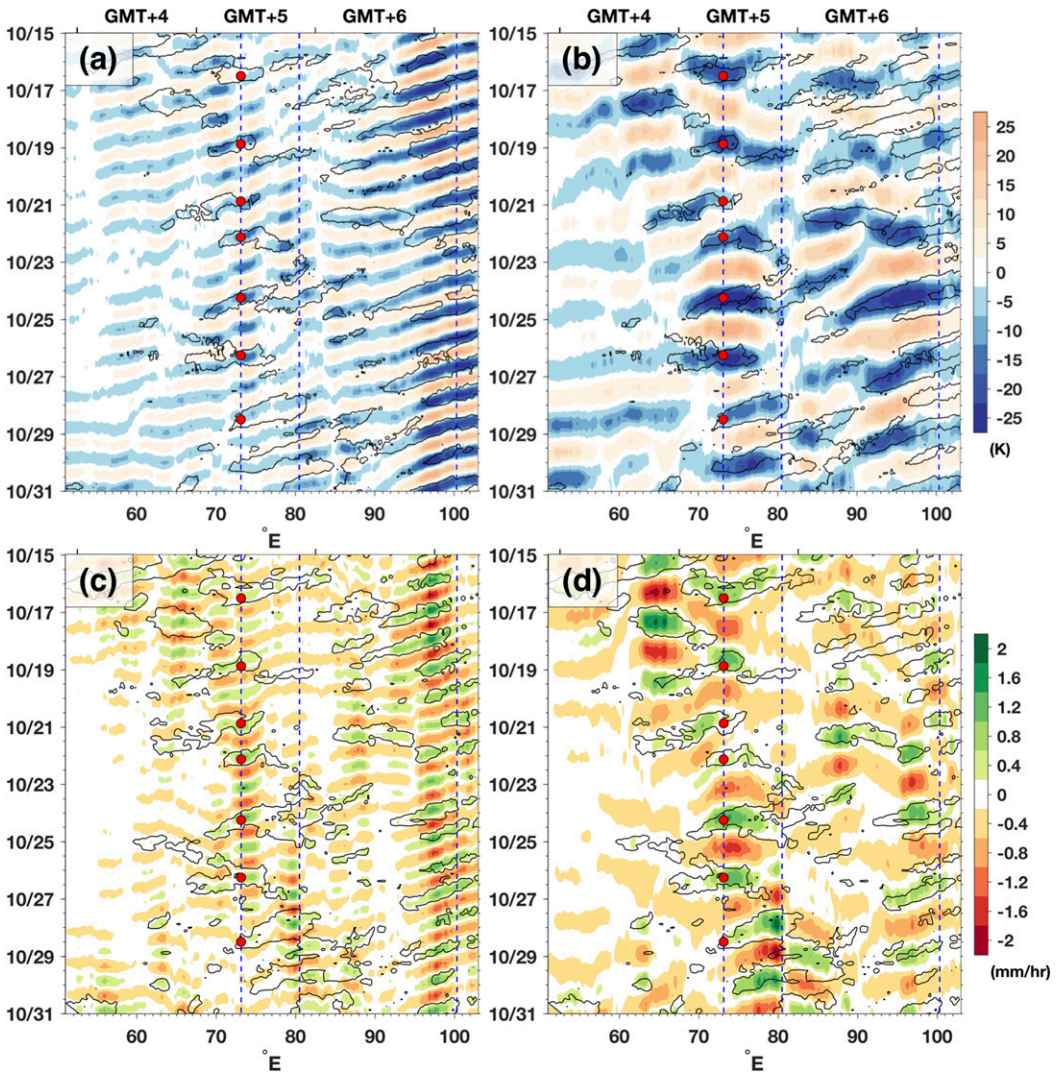

FIG. 6. (a),(b): Time–longitude diagrams of the filtered IRBT variations with (a) diurnal periodicity (0.9–1.2 days) and (b) quasi-2-day periodicity (1.6–3 days) during MJO1. The black contours in both panels indicate the unfiltered averaged IRBT < 240 K. (c),(d) As in (a) and (b), respectively, but for the filtered TRMM rain-rate variations. The black contours here indicate the unfiltered averaged TRMM rain rate >1 mm h^{-1}. In all panels, the blue dashed lines, from left to right, indicate the longitudes of sites at Gan Island (73.15°E), R/V *Revelle* (80.5°E), and Padang on Sumatra (100.35°E). The red dots along the longitude of Gan Island indicate the time of convective events listed in Table 1. The ordinate is the date time in UTC (0000 UTC), and the upper abscissa is the local time zone to UTC.

shown in Figs. 2b and 2c. Note that the time difference between minima in the diurnal signal ranged from 24–27 h in Fig. 2b because of the width of the diurnal filter allowing frequencies between 0.9 and 1.2 days to be retained. Having about half the amplitude of the quasi-2-day signal, the diurnal signal tends to grow then wane as the MJO convective envelope passes.

By applying these filters along each longitude during MJO1, Fig. 6 shows time–longitude diagrams of averaged IRBT and TRMM rain rate within 1.5° latitude north and south of Gan for the diurnal (Figs. 6a,c) and quasi-2-day (Figs. 6b,d) signals. The equatorial diurnal convective signals were stronger near Sumatra than over the open ocean, indicating the dominant strong diurnal forcing of convection by topography. The cloud signals accompanied by a precipitation signal originated daily from the terrain of Sumatra in the late afternoon (1600–1800 LT) and propagated westward over the IO owing to the dominant background easterlies near Sumatra (Yanase et al. 2017).

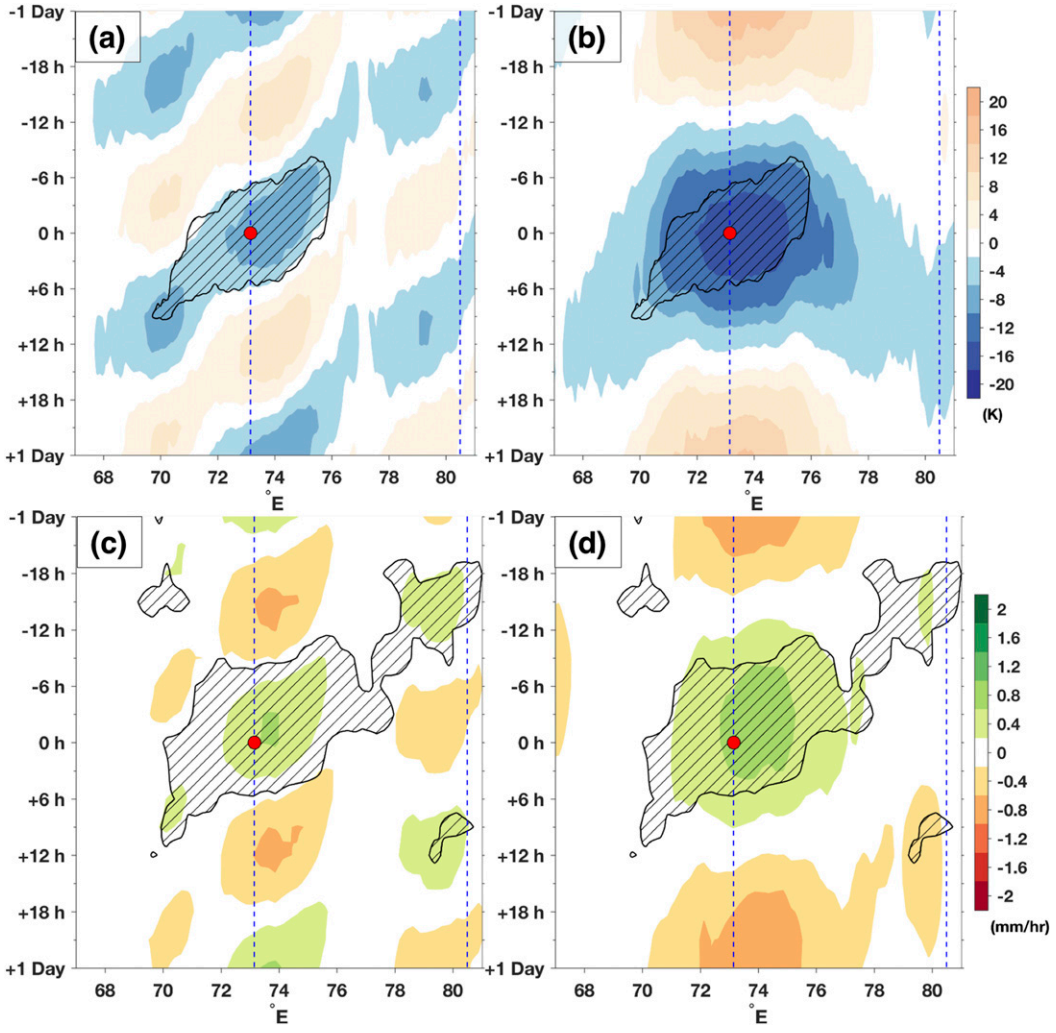

FIG. 7. As in Fig. 6, but for the seven convective events composites. The black hatched contours indicate (a),(b) the unfiltered average IRBT composite <240 K and (c),(d) the unfiltered average TRMM rain-rate composite >1 mm h^{-1}. Red dots in all subfigures denotes 0 h for the quasi-2-day events.

As the diurnal convective signal propagated westward away from the terrain, it gradually weakened over the IO. Another group of relatively strong diurnal signals appeared across the DYNAMO ESA as part of the MJO1 convective envelope, though not apparently linked to the diurnal signal coming off Sumatra. While the source of this separate regime of diurnal convection is difficult to ascertain, radiative effects were undoubtedly playing a prominent role (Gray and Jacobson 1977; Randall et al. 1991; Chen and Houze 1997). The gradual advance in the timing of the peaks in the diurnal signal at Gan (Fig. 2b) is generally consistent with the slow eastward drift in the origins of the diurnal signals across the ESA (Fig. 6a). Correspondingly, the peaks in the quasi-2-day signals advance slowly with time as well (Fig. 2c).

The IRBT and TRMM rain-rate signals associated with quasi-2-day periodicity (Figs. 6b,d) exhibited starkly different behavior patterns from the diurnal signal. First, the convectively active quasi-2-day signal was prominent over the IO in addition to near Sumatra terrain at 100°E. Second, and more importantly, the quasi-2-day signal did not always propagate as the diurnal signal. In fact, the quasi-2-day convective signals over the central IO occasionally exhibited no propagation and at times even eastward propagation during MJO1 in contrast to its diurnal counterpart, which almost always propagated east to west. In addition to these features, the active quasi-2-day signal displayed a larger amplitude over a relatively large zonal scale (up to 1000 km), and at times during MJO1 appeared as a ''checkerboard-like pattern'' with alternating areas and periods of

enhanced and suppressed convection and clouds (e.g., in Fig. 6b from 15 to 20 October between 60° and 75°E, and from 22 to 25 October between 70° and 100°E). Interestingly, the 2-day signals over Gan appeared in most instances to extend only to the eastern boundary of the DYNAMO sounding arrays (80°E) and were mostly disconnected with 2-day variability farther east, even as the active phase of MJO1 progressed through the region. This behavior is generally consistent with earlier findings in the IO during MISMO (Yamada et al. 2010) but is in contrast with the behavior of 2-day disturbances in the WPAC, which tend to progressively migrate eastward with the overall MJO convective envelope (Nakazawa 1988).

Worth noting in Figs. 6c and 6d is that the heavy rainfall ($>1\,\mathrm{mm\,h^{-1}}$) of the seven quasi-2-day convective events over the DYNAMO ESA only occurred when both the diurnal and quasi-2-day signals were convectively active, hence the quasi-2-day intervals of occurrence as shown in Fig. 3. On the other hand, the rainfall near Sumatra (90°–100°E) corresponds well to the diurnal signal, but not necessarily to the quasi-2-day signal (Fig. 6d), suggesting that the precipitation over the eastern IO was dominated by the terrain-induced diurnal convective activity, while other factors controlled the rainfall patterns over the central IO.

These differences between quasi-2-day and diurnal signals are further demonstrated in time–longitude composite diagrams (Fig. 7) for the seven convective events during MJO1. As evident from Fig. 7, the quasi-2-day convective events associated with significant precipitation over Gan occurred when the diurnal and quasi-2-day signals were both convectively active. The active diurnal signal propagated westward through the DYNAMO arrays (Figs. 7a,c) with an estimated propagation speed of $\sim$10–12 $\mathrm{m\,s^{-1}}$, which largely explains the propagation speed of the convective events shown in Fig. 4. In contrast, the quasi-2-day active signals appeared almost stationary, and the convective signals possessed a zonal scale up to about 1000 km (Figs. 7b,d), a likely result of broadening stratiform clouds. In addition to the considerable amount of spatial range of the active clouds and significant precipitation, the quasi-2-day composite signal contributed 54.7% of the variance in cloud activity (43.5% in precipitation) over Gan during MJO1.

As inferred from the above analyses, the quasi-2-day convective events observed over Gan during MJO1 were actually composed of at least two modes of convective activity. One was the westward-propagating diurnal convective waves corresponding to the $n = 1$ westward-propagating IGWs with phase speed of 10–12 $\mathrm{m\,s^{-1}}$ (Takayabu 1994a,b; Takayabu et al. 1996; Haertel and Kiladis 2004; Wheeler and Kiladis 1999). The other was the near-stationary quasi-2-day convective disturbances with zonal scale up to $\sim$1000 km, which contributed approximately half of the convective variance over Gan during MJO1. Overall, the combination of both modes contributed substantially—67% to the variance of cloud activity over Gan during MJO1 (and about 65% in TRMM rain-rate variance). As a result, the propagation of cloud clusters in the seven quasi-2-day convective events was regulated by diurnally excited convective waves while the intensity and spatial range varied in quasi-2-day intervals.

To estimate the equivalent depth of the westward-propagating diurnal convective waves, we follow a similar approach to that taken in Takayabu (1994b). From Fig. 7a we estimate the zonal scale of the diurnal disturbance to be $\sim 1.05 \times 10^6$ m (or zonal wavenumber 38). The intrinsic frequency ($\omega_{\mathrm{int}} = \omega_{\mathrm{abs}} - kU$) is computed using $\omega_{\mathrm{abs}} = 2\pi/(1\ \mathrm{day})$, $k = -2\pi/(1.05 \times 10^6\,\mathrm{m})$, and the zonal wind $U = 3.25\,\mathrm{m\,s^{-1}}$ (taken as the 850-mean hPa at Gan for the period of interest), which results in $\omega_{\mathrm{int}} = 9.22 \times 10^{-5}\,\mathrm{s^{-1}}$ (or 1.27 cycles per day). These wave characteristics coincide with the dispersion curve for a westward-propagating $n = 1$ IGW with an equivalent depth of $\sim$20 m (Fig. 8). Also shown here is the result from Takayabu 1994b for the 2-day disturbance they analyzed using TOGA COARE observations. Despite the differences between the zonal and temporal scales of the disturbances in these studies, both waves have a similar equivalent depth of $\sim$20 m.

The quasi-2-day-filtered signals in Figs. 6 and 7 also show at times a checkerboard-like pattern. This feature seen in the cloud and rainfall analyses could be interpreted in terms of the counterpropagating convective signals seen during MISMO, which interacted to enhance rainfall locally on a 2–4-day time scale (Yamada et al. 2010, their Fig. 15). In a few of the 2-day events depicted in Fig. 3, it appears that an eastward-propagating convective signal west of Gan encountered a westward-propagating signal enhancing rainfall in the vicinity of Gan. The environmental wind structure (i.e., low-level westerlies underlying upper-level easterlies seen in Fig. 12c) during MJO1 would support Yamada's mechanism of counterpropagating convective signals.

In addition to Yamada's mechanism, Chen and Houze (1997, their Figs. 19a,b) using TOGA COARE observations, showed that the conceptual "diurnal dancing" process accounts for a checkerboard pattern of convective systems and a 2-day cycle of cloud activity at a given longitude. More precisely, Chen and Houze (1997) explain the observed cloud variability in terms of "a combination of 2-day IGWs and the diurnal dancing" (their Fig. 19b). In contrast to their findings, our analyses suggest that the quasi-2-day convective events during

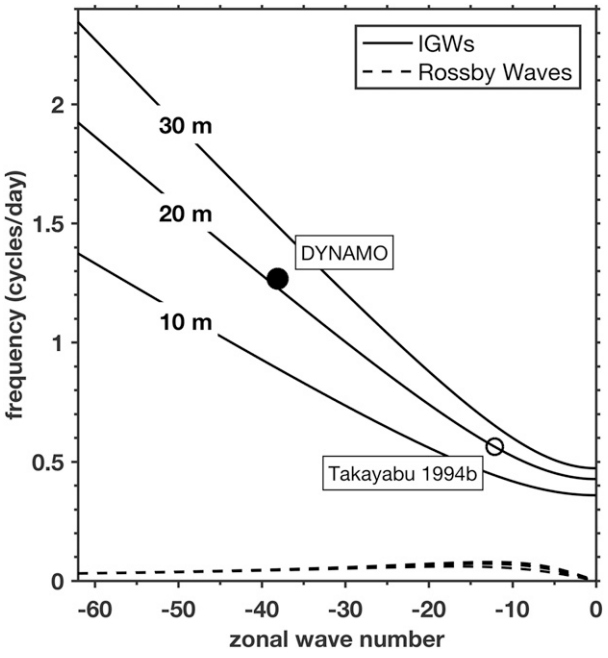

FIG. 8. Dispersion diagram with an estimated characteristic value of the propagating diurnal signals within the seven quasi-2-day convective events obtained from the composite during DYNAMO (black dot), and that estimated in Takayabu (1994b) (black circle). Similar to Fig. 8 in Takayabu (1994b), the dispersion curves indicate the $n = 1$ westward-propagating IGWs (solid) and $n = 1$ Rossby waves (dashed) with the equivalent depths of 10, 20, and 30 m, respectively.

MJO1 were composed of westward-propagating diurnal convective disturbances and a quasi-2-day modulation of that convective signal as shown in the composite analyses. That is, the 2-day IGWs were not necessarily a component for the propagating feature in these seven events, at least within the longitudes of the DYNAMO arrays. Instead, the diurnal convective waves controlled the propagation while those diurnal signals were modulated on a quasi-2-day time scale. Later analyses will show that the quasi-2-day periodicity is likely related to the life cycle of the convective systems and associated boundary layer modification and recovery.

Maps in Fig. 9 show where these two convective modes (diurnal and quasi-2-day) were most active during MJO1. The quasi-2-day convective disturbances (Fig. 9a) preferentially occurred over open ocean and were mostly confined to near the equator between 10°N and 10°S, similar to that observed over the WPAC during TOGA COARE (Fig. 7 in Haertel and Johnson 1998), and the disturbances were present throughout the DYNAMO ESA maximizing near Gan during MJO1. On the other hand, the stronger diurnal disturbances (Fig. 9b) were closely tied to the terrain of Sumatra, southern India, and the coast of Sri Lanka, being about half the amplitude of the quasi-2-day disturbances over the central IO (Figs. 2b,c).

In general, compared to the diurnal variances, the quasi-2-day variances in IRBT (Fig. 9c) and in TRMM rain rate (Fig. 9d) were larger over the central equatorial IO and smaller near the coast of Sumatra. The differences between the quasi-2-day and diurnal variance in TRMM rain rate were smaller than those in IRBT. It is unclear at this point why the amplitude of the quasi-2-day variance was so large in proximity to Gan during DYNAMO, but it may be related to the MJO1 initiation over the central IO.

To determine how the DYNAMO results compare to other years, a climatology of quasi-2-day and diurnal variability using IRBT data is investigated for the October–December periods from 1998 to 2012 (15 years). Similar patterns of the variances are found for this longer period (Fig. 10). The quasi-2-day disturbances preferentially occurred over the IO while the diurnal disturbances were closely tied to the terrain of Sumatra, southern India, and the coast of Sri Lanka, showing smaller amplitudes over the ocean. Interestingly, for reasons not yet investigated, the stronger quasi-2-day signals in the central IO as during DYNAMO are also observed in certain years, for example, 1999, 2000, 2006, 2007, 2009, and 2012 (not shown). During other years, the stronger quasi-2-day signals are observed closer to the eastern IO as in the averaged pattern (Fig. 10).

Given the large variance in the 2-day signals near Gan, observations from that island should provide insight into the structure of the quasi-2-day convective disturbances. With the aid of the various observational platforms deployed at Gan (radiosondes, AMIE-Gan large-scale objective analyses, and CombRet dataset), the vertical structures of the quasi-2-day convective disturbances are examined in the next section.

6. Composite features of quasi-2-day convective disturbances

Figure 11 shows 48-h-window composites of cloud-top population and rain rate over Gan. The composites are centered at 0 h, as this time represents a minimum in IRBT, which from Fig. 2 can be seen to be distributed throughout the diurnal cycle. The atmospheric cloudiness shows a clear oscillation with a period of 2 days in which different stages of cloud activity can be identified. During the first stage of the oscillation from −1 day to −9 h, the cloud tops were generally low and mostly confined to below 700 hPa, indicating the convectively suppressed stage of the disturbances. Starting from −9 h, the composite cloud tops rose and

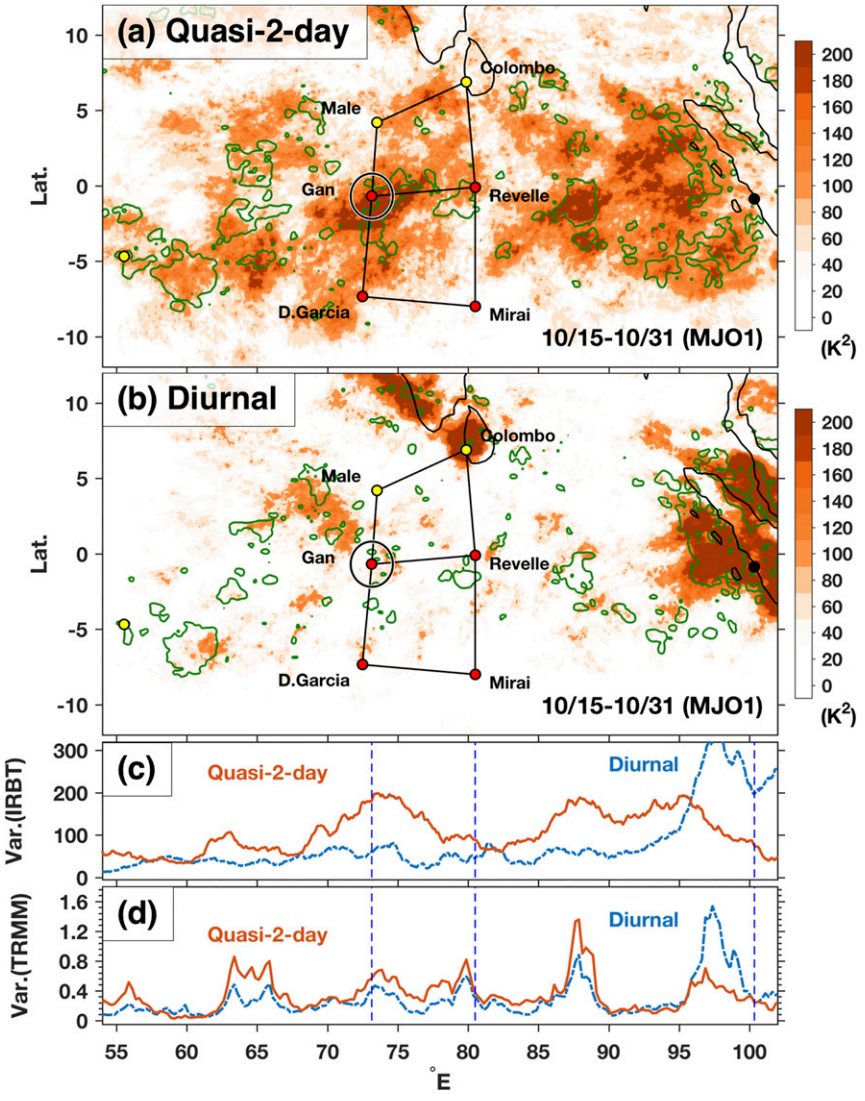

FIG. 9. Maps of IRBT and TRMM rain-rate variances over tropical IO during MJO1 for (a) quasi-2-day (1.6–3 days) and (b) diurnal (period of 0.9–1.2 days) periodicity. The colored regions indicate the IRBT variance, the green contours indicate the TRMM rain-rate variance $>0.64\,\mathrm{mm^2\,h^{-2}}$. (c) The mean variances of IRBT over 150 km north and south of Gan during MJO1. The red (blue) curve indicates the quasi-2-day (diurnal) variance as a function of longitude, and the blue vertical dashed lines indicate, from left to right, the longitudes of Gan Island, R/V *Revelle*, and Padang on Sumatra. (d) As in (c), but for the mean variances of TRMM rain rate.

the mean rainfall increased, indicating intensifying convection. Heavier rainfall commenced near −6 h and the composite rain-rate peak occurred before 0 h. It is reasonable that heavier rain occurred when deep convective clouds were dominant in the convective events prior to their mature stage. Although the satellites are incapable of detecting shallow clouds beneath thick higher clouds, the broadening cloud-top population suggests the coexistence of different cloud tops besides the dominant deep convective clouds during this stage. This convective intensifying stage was similar to that observed and identified as the ''initial convective tower stage'' in Takayabu et al. (1996) with TOGA COARE observations. The rainfall retrieved from SMART-R was lighter and the peak occurred earlier than that from TRMM. This is consistent with findings of Xu and Rutledge (2014) based on radar data from the R/V *Revelle*, where they found that TRMM 3B42 product overestimates rainfall during convectively active periods, likely due to the abundance of high cloudiness.

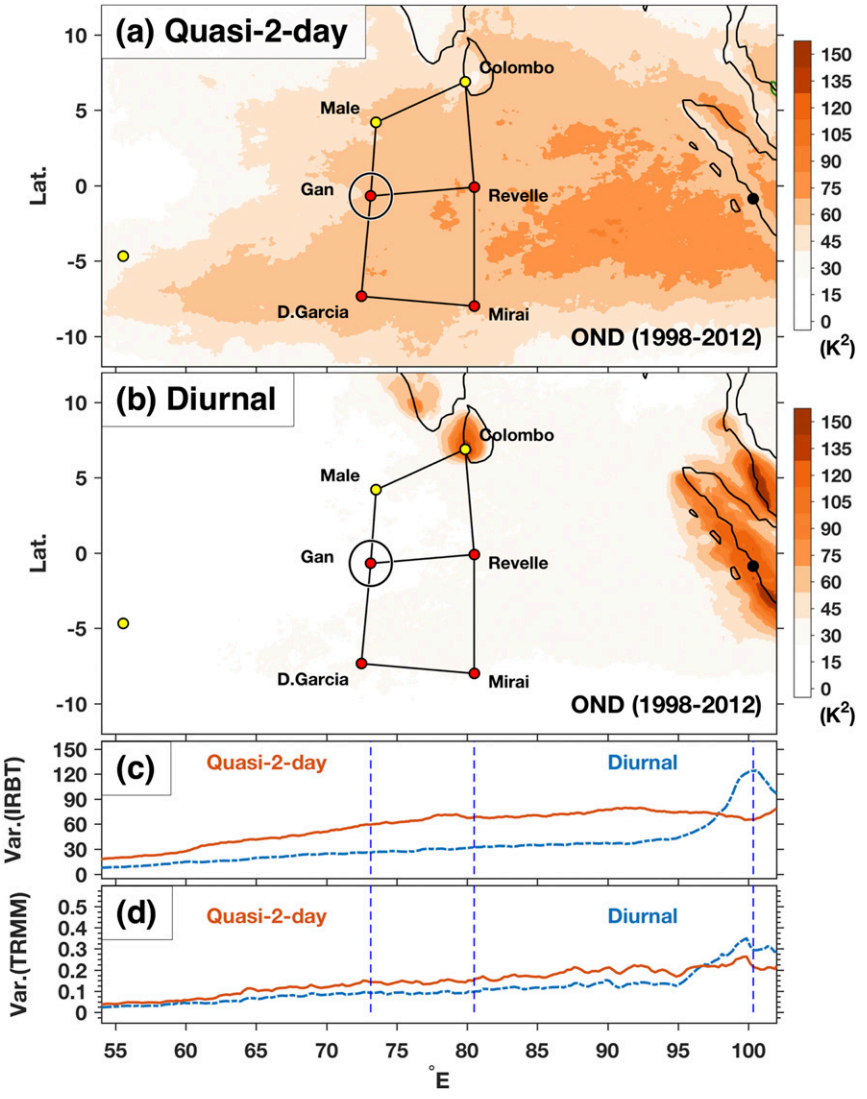

FIG. 10. As in Fig. 9, but for the averaged variance distribution during October–December from 1998 to 2012 (15 yr) using IRBT dataset from NOAA (0.07° resolution).

At 0 h, most cloud clusters were well developed with cloud-top heights above 200-hPa (~220 K), and the quasi-2-day convective disturbances had reached their convectively mature stage while at the same time the mean IRBT showed a minimum peak. After 0 h the average rain rate decreased and the dominant cloud tops dropped slightly to near 200 hPa (220–240 K) from +3 to +6 h, likely a result of trailing stratiform anvils (Takayabu et al. 1996; Chen and Houze 1997; Haertel and Johnson 1998; Zuluaga and Houze 2013). From +6 to +18 h, the convective components of the quasi-2-day disturbances had mostly decayed around Gan, with light rain and dominant cloud tops between 250 and 270 K for nearly 12 h.

Four stages in the life cycle of the quasi-2-day convective disturbances over Gan during MJO1 can thus be identified in terms of cloud activity: suppressed, convective intensifying, mature, and stratiform. This is similar to the observations of TOGA COARE (Takayabu et al. 1996; Haertel and Johnson 1998) and is consistent with the ''building block'' life cycle of MCSs proposed by Mapes et al. (2006).

Basic fields from Gan radiosondes of the quasi-2-day life cycle of convective disturbances are shown in Fig. 12. In the suppressed stage, the atmosphere was relatively dry with moisture accumulating within the BL (maximum near −12 h as shown in Fig. 12a). Moisture then deepened and became abundant throughout the troposphere as the convection developed. The temperature

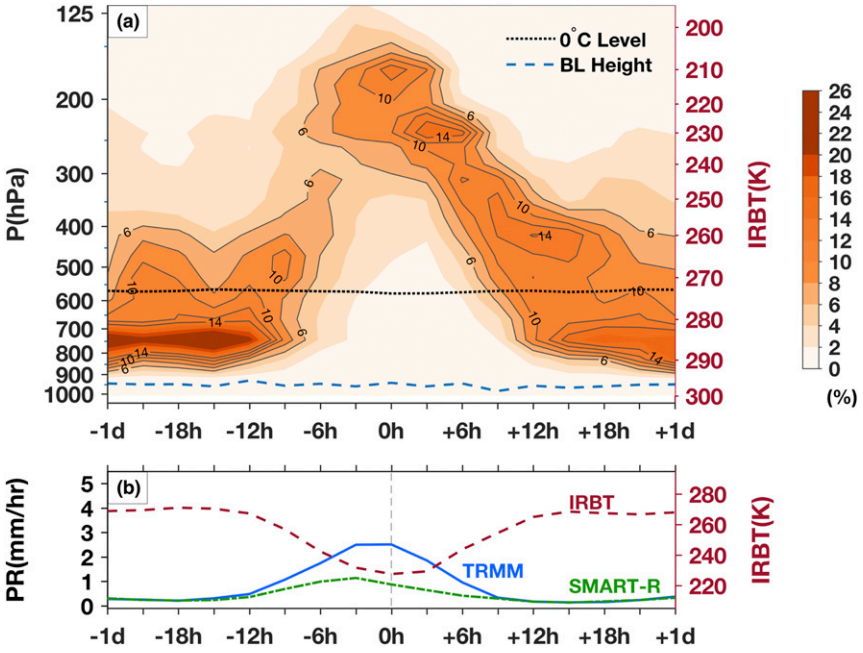

FIG. 11. The 48-h window composites for the quasi-2-day convective events. (a) Composite IRBT areal percentage calculated as in Fig. 2. Black solid contours indicate values from 6% to 14% with intervals of 2%. The black dotted line near 600 hPa (blue dashed line near 950 hPa) indicates the period-mean 0°C-level height (boundary layer height) calculated from Gan radiosonde. The boundary layer heights in the composite analysis are based on mixed-layer depths reported in Johnson and Ciesielski (2017). (b) Averaged IRBT (red dashed), averaged TRMM rain rate (blue solid), and adjusted SMART-R surface rain rate (green dash–dotted) over Gan. The vertical gray dotted line indicates 0 h.

field (Fig. 12b) shows warm anomalies beginning at low levels near −1 day then ascending after −18 h and during the intensifying stage, presumably associated with the cloud development from shallow cumulus to deep convective clouds (supported by Q_1 and Q_2 profiles, shown later in Fig. 14). Meanwhile, the BL was relatively warm prior to the onset of heavier rainfall near −9 h and relatively cool during the heavy rain period for ~18 h.

At 0 h, the atmosphere was moistest throughout the troposphere as the quasi-2-day convective disturbances reached their mature stage. From 0 to +6 h, in addition to the warm cores in the convective towers (400–200 hPa), a cool anomaly appeared near and above the 200-hPa level. This feature is coincident with cloud-top radiative cooling shown in Fig. 13. A second cool anomaly is evident below 500 hPa, with a peak directly below the 0°C level, due to the melting and evaporative cooling. While moisture was abundant above the 0°C level, the lower troposphere began to dry after +3 h. Also after the mature stage, the lower troposphere became relatively warm from +6 to +18 h in the 900–700-hPa layer. These are likely signatures of mesoscale downdrafts, which also caused "onion type" profiles in the soundings during the stratiform stage (Zipser 1977). However, cool anomalies still existed in the BL around +12 h due to spreading cold pools from the evaporating precipitation. During the stratiform stage, a thin moist layer slightly below 0°C level related to the melting process under stratiform anvils (Johnson et al. 1996) can also be seen from +6 to +18 h (Fig. 12a).

The temperature variation in the BL showed a clear quasi-2-day oscillation within the 48-h window. Overall, the composite BL cool anomaly lasted for almost a day (from −9 to +12 h) during the convective intensifying and mature stages and the early stratiform stage. This long BL recovery of quasi-2-day disturbances over Gan during DYNAMO supports the idea that convective processes during the stratiform stage can be a key factor for the quasi-2-day periodicity observed in the disturbances, similar to the processes in MCSs observed during TOGA COARE in WPAC (Takayabu et al. 1996; Chen and Houze 1997).

The zonal wind field (Fig. 12c) shows strong westerlies in the lower troposphere below 700 hPa with easterlies above during this active period of the quasi-2-day disturbances (Zhang and Yoneyama 2017). Prior to the mature stage, a westerly anomaly occurred in the lower

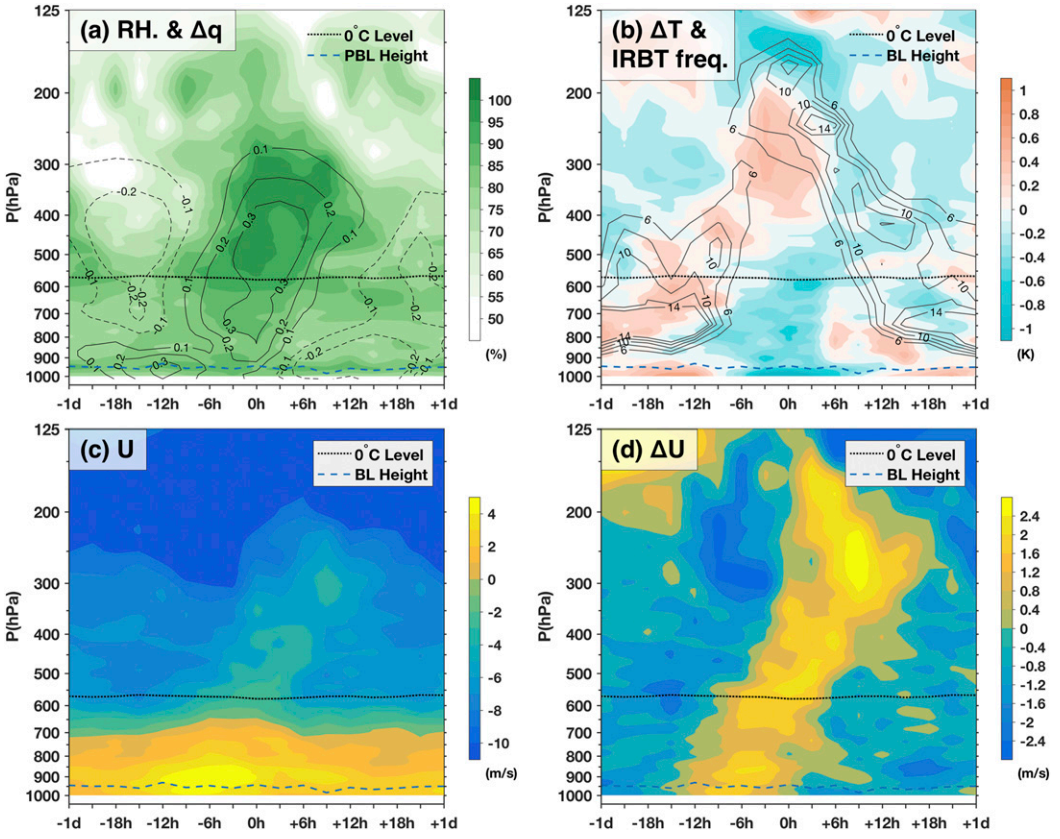

FIG. 12. The 48-h-window composites for the quasi-2-day convective events. (a) RH from Gan radiosonde (colored) with respect to ice for $T < 0$°C and water vapor mixing ratio (q) anomaly from AMIE-Gan objective analysis (g kg^{-1}; positive values in black solid contours and negative values in black dashed contours). (b) The temperature anomaly (K; colored) from radiosonde at Gan, and the black contours indicate the IRBT areal percentage from 6% to 14% as in Fig. 11a. (c) The zonal wind (m s^{-1}) and (d) the zonal wind anomaly (m s^{-1}) from radiosonde at Gan. Anomalies were computed by subtracting the MJO1 time-period mean from the composite fields. The period-mean 0°C-level height and the boundary layer height in each panel are as in Fig. 11.

troposphere (1000–800 hPa) near −6 h (Fig. 12d). This westerly anomaly then shifted upward as the quasi-2-day convection developed with a peak in the upper troposphere (200–300 hPa) near +9 h. This result suggests an upward transport of westerly momentum associated with the quasi-2-day convective disturbances over Gan during MJO1. These zonal wind anomalies are consistent with low-level convergence prior to 0 h and upper-level divergence centered around 0 h to support deep convection during this period (see Fig. 14). There is evidence from Figs. 11d and 13a of a downward transport of easterly momentum within stratiform precipitation regions of the disturbances (from +6 to +18 h), consistent with the TOGA COARE Doppler radar analyses of Houze et al. (2000), which show the existence of such transport in what they call the ''westerly onset region'' of the MJO Kelvin–Rossby circulation. Liu and Wang (2012) have argued that easterly momentum transport by 2-day waves serves to slow down and convectively enhance moist Kelvin waves or the MJO, so such transports may play an important role in the life cycle of the MJO itself.

The radiative impacts of clouds and moisture to the quasi-2-day convective disturbances are considered in Fig. 13 with composites of total (Q_R), LW, and SW cloud radiative forcings (CRFs) obtained from the CombRet dataset. The total cloud radiative cooling (Fig. 13a) maximized at upper levels above 200 hPa at 0 h as a result of the strong cloud-top longwave cooling, with peak rates approaching 5 K day^{-1} (Fig. 13b). The CRF SW heating profiles (Fig. 13c) show large peaks directly beneath the cloud tops near 200 hPa (Webster and Stephens 1980) in the −6 to 0 h timeframe. Presumably, these large heating rates are related to the events with 0 h occurring during the daylight hours when SW effects would be present (see Fig. 2 for local times of 0-h occurrences). For these cases, this upper-level SW heating peak would promote a stabilization of the lapse rate

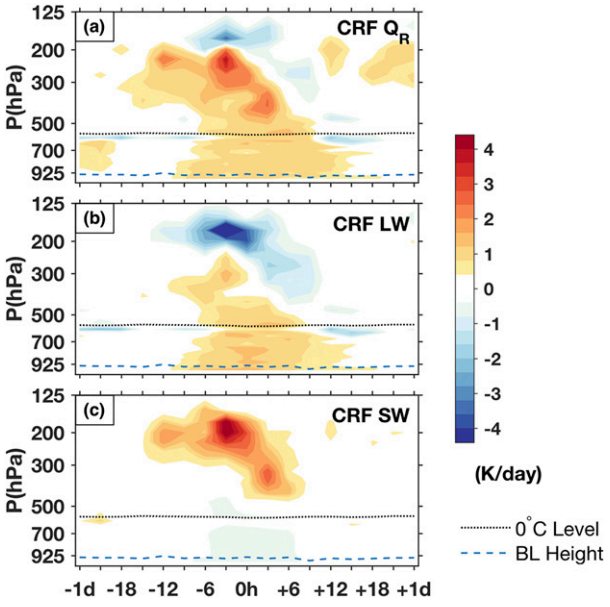

FIG. 13. As in Fig. 12, but for the variations of CRFs (K day^{-1}) from the CombRet dataset. (a)–(c) The total cloud radiative heating rate (Q_R = LW + SW), the LW cloud heating rate, and the SW cloud heating rate, respectively. The period-mean 0°C-level height and the boundary layer height in each panel are as in Fig. 11.

and a weakening of the deep convection (Randall et al. 1991) that would also enhance midlevel convergence and upper-level divergence (Gray and Jacobson 1977), thereby assisting the transition to stratiform precipitation. During the mature stage, the CRF composites show a slight downward-sloping pattern in the upper troposphere as a result of the trailing stratiform clouds, similar to the squall line structure found in Johnson et al. (1990). From the intensifying stage to the stratiform stage, CRF LW heating in the lower troposphere was dominant from −9 to +18 h.

Although the cloud radiative forcings are prominent as the quasi-2-day convection intensifies and reaches its mature stage, fewer impacts are observed during the stratiform stage after +6 h. To better understand the structure and variation of the quasi-2-day convective disturbances, we make use of AMIE-Gan large-scale objective analysis data to investigate the convective features during MJO1. Although the dataset is representative of the region with only a 150-km radius around Gan, considering the propagation speed (10–12 m s^{-1}) and the zonal scale (~1000 km) of the quasi-2-day events, it is capable of sampling variability within the quasi-2-day convective disturbances.

Figure 14 includes the 48-h-window composites for horizontal wind divergence and large-scale vertical motion, apparent heating Q_1, and apparent drying Q_2 from AMIE-Gan objective analysis. During the convective intensifying stage (from −9 to 0 h) upward motion, associated with low-level convergence and upper-level divergence, dominated the troposphere with a maximum around 600 hPa (Fig. 14a). As the convection matured, the updrafts shifted upward, and low-level downdrafts due to stratiform precipitation dominated over the updrafts. Low-level divergence maximized in the BL during the mature stage (after +3h), similar to the findings of Zuluaga and Houze (2013). In the mature stage and later in the stratiform stage, a separate peak in updrafts was present above 0°C level while mesoscale downdrafts dominated the lower troposphere as generally observed in other stratiform regions (Cifelli and Rutledge 1994; Uyeda et al. 1995).

Starting from −9 h, positive Q_1 was observed throughout the troposphere with a maximum between 600 and 500 hPa around −6 and −3 h, which then transitioned to near 400 hPa at 0 h (Fig. 14b). The principal Q_2 peak was found below the 600-hPa level with maximum at −3 h (Fig. 14c) when the highest rain rate occurred (Fig. 11b). The results are consistent with Yanai et al. (1973) that the vertical separation of the Q_1 and Q_2 peaks is indicative of strong convective eddies fluxes which prevailed during the convective intensifying stage from −9 to 0 h (Fig. 14d).

After 0 h, the principal Q_1 peak shifted upward above the 0°C level between the 500- and 300-hPa levels while negative Q_1 was prevalent below the 0°C level from +3 to +15 h. In Q_2 positive peaks occurred above the 400-hPa level around +9 h, with negative values found mostly below the 700-hPa level from +6 to +18 h. These results reflect the typical top-heavy signatures of stratiform precipitation in which stronger heating and drying occur in the upper troposphere while cooling and moistening due to melting and evaporation occur in the lower troposphere (Johnson 1984; Houze 1989, 1997). There is an upward shift in the MSF flux during the developing stages of the quasi-2-day disturbances (Fig. 14d), with another peak in the stratiform stage at +6 h. This latter feature likely reflects the remnant convective components that occurred after 0 h in some of the events as seen in NCAR S-Pol data (not shown).

The disturbance composite equivalent potential temperature (θ_e) anomaly field is shown in Fig. 15a. From −18 to −6 h, the atmosphere was unstable with higher θ_e in the BL as deep convection starts to develop. At −6 h, θ_e in the BL transitioned from relatively high to relatively low as the rain became heavier. Afterward, the lower troposphere (900–700 hPa) gradually became more stable with low θ_e during the mature stage due to a transport of low θ_e by downdrafts (e.g., Zipser 1977). The low BL θ_e lasted for almost 18 h (from −6 to +12 h)

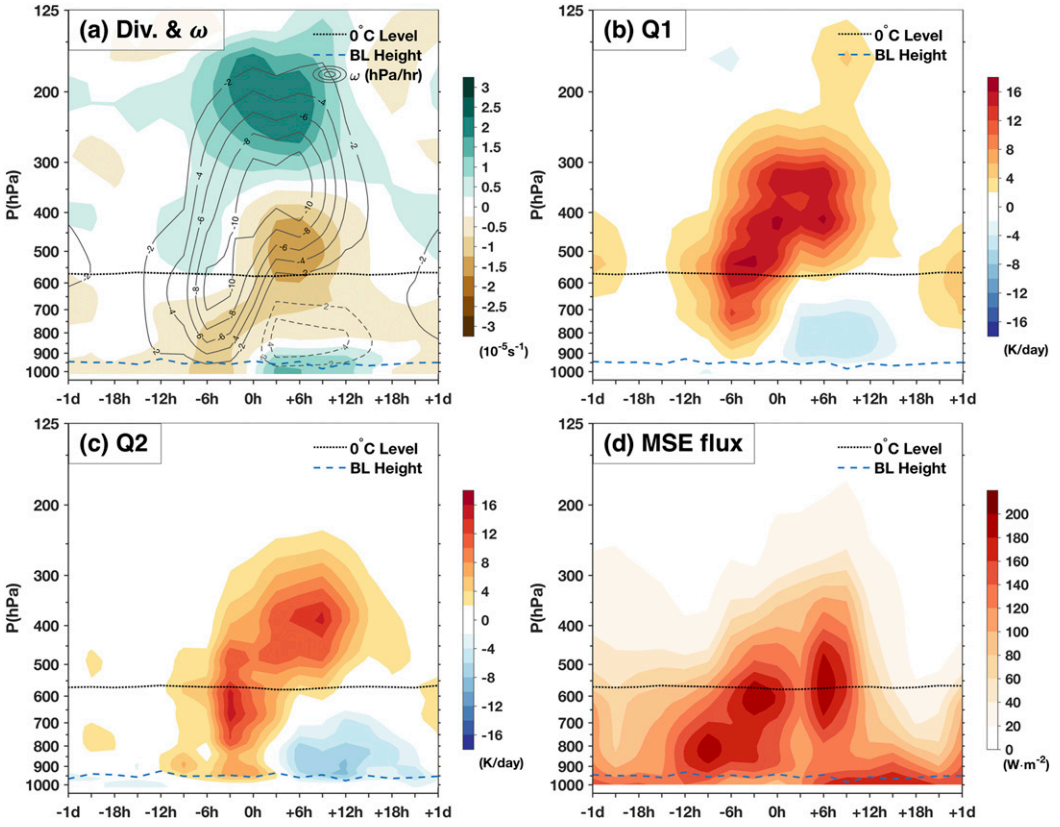

FIG. 14. As in Fig. 12, but for the variations of (a) the horizontal wind divergence (colored; $10^{-5}\,s^{-1}$) and the vertical motions (hPa h^{-1}; upward motions in solid contours and downward motions in dashed contours), (b) the apparent heating Q_1 (K day^{-1}), (c) the apparent drying Q_2 (K day^{-1}), and (d) the vertical eddy flux of moist static energy (MSE; J $m^{-2}\,s^{-1}$) calculated from AMIE-Gan large-scale objective analysis and CombRet dataset. The period-mean 0°C-level height and the boundary layer height in each panel are as in Fig. 11.

in the life cycle of the disturbances. The prevalent, long-lasting stable BL over Gan, a result of the convective process during the stratiform stage, impacted the recovery of the lower troposphere and the occurrence of the next round of convection over that region, similar to the convective processes during TOGA COARE in WPAC (Takayabu et al. 1996; Chen and Houze 1997).

The atmospheric stable layers based on Gan radiosonde data also show variation over the life cycle of the quasi-2-day convective disturbances (Fig. 15b). Tropical convection often shows a trimodal structure in the vertical profiles of cloud population, divergence, and cloud detrainment (Johnson et al. 1999). This structure suggests the impact of three major stable layers of the tropical atmosphere from top to bottom: the tropopause inversion layer, the melting stable layer near 0°C level, and the trade-wind stable layer in the lower troposphere (Schubert et al. 1995; Johnson et al. 1996, 1999; Kikuchi and Takayabu 2004). During MJO1 the trimodal structure is clearly identified from the temperature lapse-rate profiles. The tropopause inversion layer occurred mostly above 125 hPa except during the mature stage when gravity wave features excited by the MJO convective envelope lead to its lowering (Johnson and Ciesielski 2013). The melting stable layer generally occurred near and slightly above the 0°C level and was strongest during the mature and stratiform stages when the melting process was most prevalent over large areas.

A trade-wind-like stable layer is observed between 700 and 900 hPa with a more complex variation than the other two layers. Previous modeling studies have suggested that the overall height of the trade-wind stable layer is controlled by both local thermodynamic processes (Albrecht et al. 1979; Sarachik 1985) and large-scale dynamical adjustment across different latitudes (Schubert et al. 1995). Over the temporal scale of ~2 days, it appears that local processes played a dominant role in determining its height. These processes include radiative effects and moist convection, which tend to deepen the trade layer, while large-scale subsidence tends to shallow it. On average, the height of the trade stable layer was near 800 hPa throughout MJO1, but

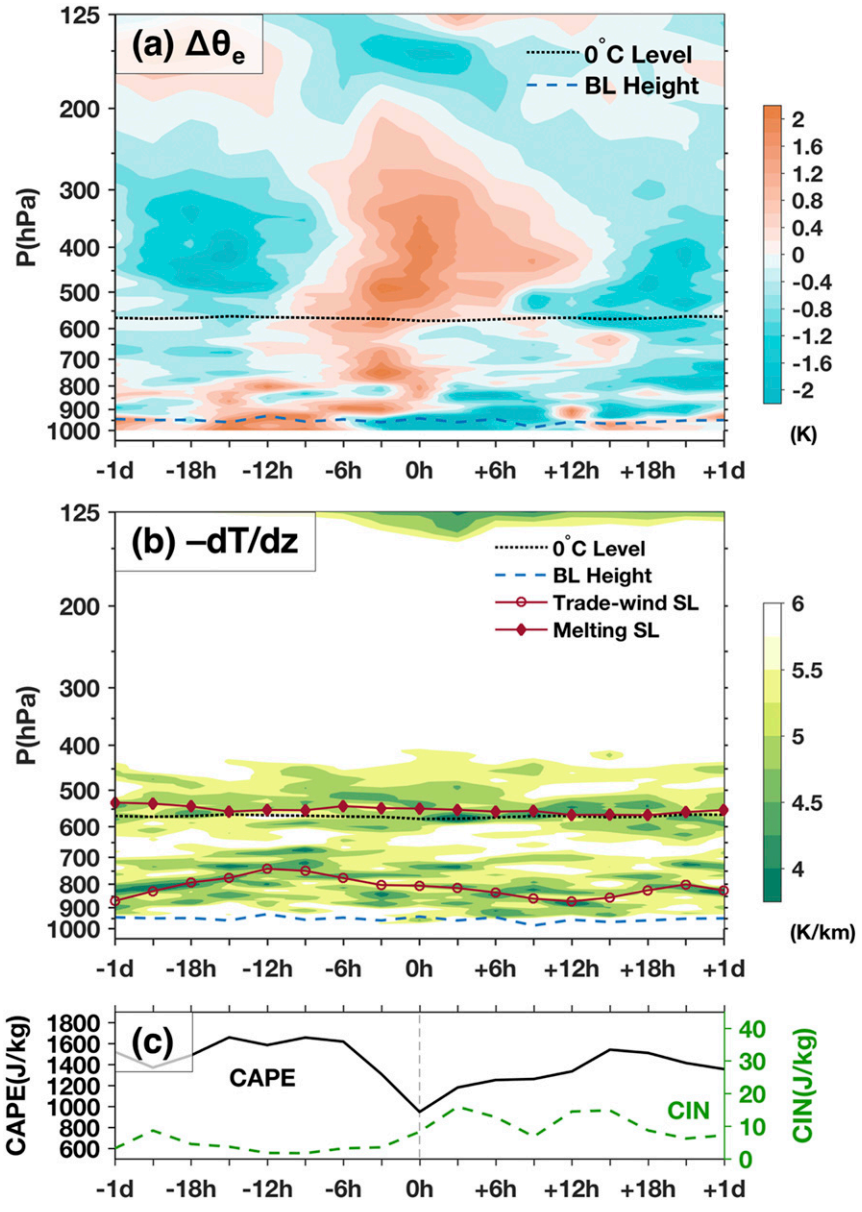

FIG. 15. As in Fig. 12, but for (a) the equivalent potential temperature anomaly computed by subtracting the MJO1 time period mean from the composite fields (K; colored), (b) the atmospheric temperature lapse rate (K km^{-1}), and (c) the CAPE (black solid) and CIN (green dashed) calculated from radiosonde at Gan. In (b), the average heights of the top 10% most stable levels within the melting stable layer (trade wind stable layer) are highlighted by a dark red line with diamond (circle) markers. The period-mean 0°C-level height and the boundary layer height in each panel are as in Fig. 11.

during the suppressed stage of the quasi-2-day disturbances (from −1 day to −9 h), it moved progressively upward to near 700 hPa. This period was marked by large-scale upward motion (Fig. 14a), weak cloud-top radiative cooling near 600 hPa (Fig. 13), and unstable conditions at low levels (Fig. 15a), all of which would promote a deepening trade layer. After −6 h, but particularly after 0 h, low-level subsidence, midlevel radiative warming, and BL cooling predominated, resulting in a reduction in the trade-layer depth. In the mature stage (from 0 to +6 h), the trade-layer height showed the largest variance as a result of more downdraft-induced complex temperature profiles in the lower troposphere. The trade-layer heights were generally low (~900 hPa) in the early

stratiform stage (from +6 to +12 h) as cooler BL θ_e air and subsidence dominated.

The composites of convective available potential energy (CAPE) and convective inhibition (CIN) derived from Gan sounding data are shown in Fig. 15c. Although these stability indices exhibit considerable variability among the seven cases, their composite structure is quite reasonable, with larger CAPE prior to the mature stage and a minimum at 0 h, as also shown for the composite MJO life cycle by Xu and Rutledge (2014). In contrast, the composite CIN was relatively small before the mature stage and became larger after 0 h during the mature and stratiform stages due to enhanced stability in the lower troposphere.

The composite quasi-2-day disturbance vertical heating structures, kinematic and thermodynamic fields, radiative profiles, and modification of the boundary layer suggest that these phenomena have properties resembling those of individual tropical MCSs, evolving from shallow cumulus to congestus to deep convection to stratiform precipitation (e.g., Houze 1997; Zipser 1977), as well as 2-day disturbances observed in the western Pacific (Takayabu et al. 1996; Chen and Houze 1997). Such structures and life cycle behavior are observed not only on the time and space scales of individual MCSs and quasi-2-day disturbances, but are characteristic of phenomena all the way up to the scales of convectively coupled Kelvin waves and the MJO itself (Mapes et al. 2006; Kiladis et al. 2009).

7. Interpretation of quasi-2-day convective disturbances

Previous studies of 2-day disturbances in the western Pacific (e.g., Takayabu et al. 1996; Chen and Houze 1997; Haertel and Johnson 1998) and the Indian Ocean (Yamada et al. 2010) have shed considerable light on these phenomena. Drawing upon these studies as well as the current findings reported in this paper, we offer a new interpretation of mechanisms for the quasi-2-day disturbances observed during the October MJO in DYNAMO.

As a first consideration, we relate our results to the Chen and Houze (1997) ''diurnal dancing'' paradigm. The very slow eastward drift of the origin of the diurnal signal affecting Gan ($\sim$1 m s^{-1}; Fig. 6a) differs significantly from the 10–15 m s^{-1} eastward movement illustrated in Fig. 19b of Chen and Houze (1997). According to their paper, that paradigm was based on a series of convective systems occurring during the period 11–16 December 1992. Moreover, there was mostly easterly flow with little vertical shear throughout the troposphere during that period (Chen et al. 1996), in contrast with DYNAMO, where during the October MJO there were westerlies below 700 hPa and easterlies above (Fig. 12c). This much slower eastward movement of the diurnal signal in DYNAMO yields a $\sim$1-day signal downstream to the west rather than a quasi-2-day signal, so the diurnal dancing argument that may have been relevant to the TOGA COARE period they studied does not fit the DYNAMO conditions. It is more likely that, for some reason yet to be fully understood, a diurnal signal initiates between 80° and 85°E that is separate from that coming off Sumatra,[1] moves westward at 10–15 m s^{-1}, and crosses the longitudes of Gan, where it encounters an environment that contributes to a quasi-2-day time periodicity.

In an attempt to understand the quasi-2-day signal at Gan and also put it into the perspective of convective phenomena with similar periodicity observed during MISMO as reported by Yamada et al. (2010), S-Pol data for the seven individual events have been examined (not shown, but available at https://www.eol.ucar.edu/field_projects/dynamo). Several of these DYNAMO cases exhibited eastward movement of convective cells with westward movement of stratiform anvils, similar to Yamada et al.'s findings, but other cases exhibited convective cells moving in different directions. Regardless of the motion of the convective cells, however, the stratiform anvils in each case moved from east to west due to easterly flow aloft (Fig. 12c).

Thus, a different scenario for the quasi-2-day variability is proposed. Diurnally driven convective events initiate between 80° and 85°E and move westward at 10–15 m s^{-1}, arriving at the longitude of Gan approximately 1 day later. Generally, only every other diurnal signal is amplified, leading to a quasi-2-day signal at Gan. The stabilization of the boundary layer and lengthy recovery from the first diurnal event (Figs. 11, 14) is the factor that prevents the next diurnal event from amplifying. Contributing to this prolonged stabilization, in addition to convective-scale downdrafts, are stratiform anvils that drift westward with time. These anvils, which produce light precipitation and cloud shading, cross the longitudes of Gan and modify the BL there. However, even after they pass to the west, the low-level westerlies advect the modified BL air eastward, helping to contribute to the slow BL recovery observed at Gan. Thus, the idea advanced by Chen and Houze (1997) that BL modification

[1] Preliminary analyses of possible causes suggest that the variable SST over the IO during this period may be a potential explanation for the initiation of the diurnal signal between 80° and 85°E, although thorough investigation of this possibility is beyond the scope of our study.

is a factor in the quasi-2-day periodicity is supported by our findings, though the different vertical shears and eastward speed of movement of the origin of the diurnal signals for the two periods of study in the two ocean basins argue for a different interpretation of the quasi-2-day periodicity.

8. Summary and conclusions

Convective events with a quasi-2-day periodicity were observed in the central equatorial Indian Ocean (IO) during the convectively active phase of the Madden–Julian oscillation (MJO from 15 to 31 October 2011 (MJO1) in the DYNAMO/AMIE/CINDY 2011 field campaign. Seven quasi-2-day convective events with significant convective activity were identified over Gan Island, which were analyzed with the aid of various observational platforms including radiosondes, radar, satellite, and surface observations. Properties of the convective features and the atmospheric structures of these events are summarized as follows.

1) Seven convective events were identified over Gan as westward-propagating convective episodes that moved through the central IO repeatedly in quasi-2-day intervals during the October MJO. The propagation speed of these convective signals was estimated by satellite infrared brightness temperatures (IRBTs) to be 10–12 m s^{-1}, which is similar to that observed over the equatorial WPAC during TOGA COARE (10–19 m s^{-1}; Haertel and Johnson 1998; Takayabu 1994b). However, the zonal scale of propagation was approximately 1000–1500 km, less than that found during TOGA COARE (2000–4000 km; Chen et al. 1996; Chen and Houze 1997; Clayson et al. 2002).
2) By isolating the quasi-2-day (1.6–3 day) and the diurnal (0.9–1.2 day) frequencies, spectral analyses reveal that the seven quasi-2-day convective events comprised two primary modes of convection: (i) a westward-propagating diurnal convective signal with phase speed of 10–12 m s^{-1}, very likely corresponding to an $n = 1$ westward-propagating IGWs with an equivalent depth of 20 m (Takayabu 1994a,b; Takayabu et al. 1996; Wheeler and Kiladis 1999; Haertel and Kiladis 2004) and (ii) a quasi-2-day convective signal having a ~1000-km zonal scale that modulated the diurnal signals. The latter strongly influenced the magnitude and the spatial distribution of the precipitation and contributed to over half of the cloud variance (54.7%) over Gan during MJO1.
3) The horizontal distributions of the two convective modes, as determined by IRBT variance, were different over the IO during MJO1. The quasi-2-day convective disturbances were prominent over the open ocean and near Sumatra but were confined to near the equator between 10°N and 10°S in the IO, similar to that in the TOGA COARE observations (Haertel and Johnson 1998). The convective variance on the diurnal time scale was closely tied to the terrain of Sumatra, southern India, and Sri Lanka, and possessed a much smaller amplitude and spatial scale than that of the quasi-2-day disturbances over the central IO.
4) In the 48-h window composites (−24 to +24 h) of moisture and cloud activity centered at the times of the lowest-averaged IRBT (0 h) in the 150-km region over Gan, four convective stages were identified in the life cycle of the quasi-2-day convective disturbances: (i) a convective suppressed stage (from −1 day to −9 h) with moisture confined in the lower troposphere, (ii) a convective intensifying stage (from −9 to 0 h) in which convection transitioned to dominant deep convective clouds, (iii) a mature stage (from 0 to +6 h) when convective systems were well-developed and transitioned from convective to stratiform precipitation, and (iv) a stratiform stage (from +6 to +18 h) when most of the convective elements decayed into stratiform systems dominating much of the 150-km region over Gan. This life cycle represents a similar pattern not only to mesoscale convective system (MCS) life cycles, but also to that observed on longer time scales all the way up to that of the MJO (Kiladis et al. 2009).
5) Radiative forcings and apparent heat sources and moisture sinks for the composite quasi-2-day disturbances have been determined. Top-heavy cloud radiative heating may play a role in promoting the longevity of the stratiform region after the disturbance mature stage. Diagnosed heat sources and moisture sinks are consistent with the shallow-to-deep-to-stratiform transition within the composite disturbances. The long duration of low BL θ_e air during the stratiform stage supports the notion that the life cycle of the MCSs may be an important factor contributing to the quasi-2-day periodicity of the disturbances over Gan along the lines proposed by Chen and Houze (1997).

The composite convective activity in the quasi-2-day convective disturbances during DYNAMO is similar to that depicted in the schematic diagram presented in Takayabu et al. (1996, their Fig. 19) using TOGA COARE observations. Both campaigns showed the convection to have many common features with long-lived convective systems and a rather long life cycle and duration of the stratiform stage. Some of the seven events indeed were characterized by the passage of

squall-line systems as observed from the NCAR S-Pol data at Gan (not shown).

The interpretation of the quasi-2-day disturbances within the convective envelope of MJO1, much like those originally identified by Nakazawa (1988), is that they are manifestations of westward-propagating, diurnal disturbances (likely IGWs) whose convective signal becomes modulated over the central IO on a quasi-2-day time scale, a combination of propagating diurnal IGWs, and quasi-2-day convective activity. There is evidence, in at least some of the cases, that counterpropagating cloud systems were present that owed their existence in part to strong vertical shear (westerlies at low levels, easterlies aloft), as hypothesized by Yamada et al. (2010). Composites of the quasi-2-day disturbances support the idea that the quasi-2-day intervals of occurrence may be a consequence of the longer time scale of mesoscale convective system development and boundary layer modification, a concept invoked by Chen and Houze (1997) to account for what they call diurnal dancing. However, the very slow eastward drift of the initiation locations of the diurnally driven signals over the central Indian Ocean, which moved westward and contributed to quasi-2-day convective disturbances over Gan, argues for a different interpretation of the mechanisms for these phenomena occurring during DYNAMO (described in section 7) that incorporates ideas from earlier TOGA COARE (Takayabu et al. 1996; Chen and Houze 1997) and MISMO (Yamada et al. 2010) studies.

Nevertheless, questions remain regarding a number of aspects of these phenomena. Why do quasi-2-day convective disturbances prevail during the convectively active phases of some MJOs but not others? For example, why were the disturbances so prominent over the DYNAMO array during the October MJO, but not the November MJO? What environmental conditions are needed to sustain these disturbances and what determines their horizontal scale? What roles do quasi-2-day convective disturbances play in the moistening of the atmosphere and momentum transport during the onset stage of the MJO? Further analyses with the radar data from Gan and cloud-resolving numerical simulations may help us characterize the convective structures of these disturbances and gain a better understanding of this intriguing phenomenon.

Acknowledgments. The authors gratefully acknowledge the three anonymous reviewers and would also like to thank Prof. Hiroyuki Yamada, Prof. Taro Shinoda, Prof. Kazuhisa Tsuboki, Prof. Wayne Schubert, Prof. Hiroshi Uyeda, and Prof. Shih-Hao Su for many helpful discussions. This research is supported by Ministry of Science and Technology of Taiwan under Grants MOST-106-2119-M-002-016 and MOST-104-2111-M-002-002-MY3, the Office of Naval Research under Grant N62909-15-1-2008, the National Science Foundation under Grant AGS-1360237, and the National Oceanic and Atmospheric Administration under Grant NA15OAR4310177. Datasets used herein are available from NCAR Earth Observing Laboratory (EOL) at http://data.eol.ucar.edu/master_list/?project=DYNAMO.

REFERENCES

Albrecht, B. A., A. K. Betts, W. H. Schubert, and S. K. Cox, 1979: A model for the thermodynamic structure of the trade-wind boundary layer. *J. Atmos. Sci.*, **36**, 73–89, https://doi.org/10.1175/1520-0469(1979)036<0073:MOTTSO>2.0.CO;2.

Chen, S. S., and R. A. Houze, 1997: Diurnal variation and life-cycle of deep convective systems over the tropical Pacific warm pool. *Quart. J. Roy. Meteor. Soc.*, **123**, 357–388, https://doi.org/10.1002/qj.49712353806.

——, ——, and B. E. Mapes, 1996: Multiscale variability of deep convection in relation to large-scale circulation in TOGA COARE. *J. Atmos. Sci.*, **53**, 1380–1409, https://doi.org/10.1175/1520-0469(1996)053<1380:MVODCI>2.0.CO;2.

Ciesielski, P. E., and Coauthors, 2014: Quality-controlled upper-air sounding dataset for DYNAMO/CINDY/AMIE: Development and corrections. *J. Atmos. Oceanic Technol.*, **31**, 741–764, https://doi.org/10.1175/JTECH-D-13-00165.1.

——, R. Johnson, X. Jiang, Y. Zhang, and S. Xie, 2017: Relationships between radiation, clouds, and convection during DYNAMO. *J. Geophys. Res. Atmos.*, **122**, 2529–2548, https://doi.org/10.1002/2016JD025965.

Cifelli, R., and S. A. Rutledge, 1994: Vertical motion structure in Maritime Continent mesoscale convective systems: Results from a 50-MHz profiler. *J. Atmos. Sci.*, **51**, 2631–2652, https://doi.org/10.1175/1520-0469(1994)051<2631:VMSIMC>2.0.CO;2.

Clayson, C. A., B. Strahl, and J. Schrage, 2002: 2–3-day convective variability in the tropical western Pacific. *Mon. Wea. Rev.*, **130**, 529–548, https://doi.org/10.1175/1520-0493(2002)130<0529:DCVITT>2.0.CO;2.

Duchon, C. E., 1979: Lanczos filtering in one and two dimensions. *J. Appl. Meteor.*, **18**, 1016–1022, https://doi.org/10.1175/1520-0450(1979)018<1016:LFIOAT>2.0.CO;2.

Feng, Z., S. A. McFarlane, C. Schumacher, S. Ellis, J. Comstock, and N. Bharadwaj, 2014: Constructing a merged cloud–precipitation radar dataset for tropical convective clouds during the DYNAMO/AMIE experiment at Addu Atoll. *J. Atmos. Oceanic Technol.*, **31**, 1021–1042, https://doi.org/10.1175/JTECH-D-13-00132.1.

Fu, Q., and K. N. Liou, 1992: On the correlated k-distribution method for radiative transfer in nonhomogeneous atmospheres. *J. Atmos. Sci.*, **49**, 2139–2156, https://doi.org/10.1175/1520-0469(1992)049<2139:OTCDMF>2.0.CO;2.

Gallus, W. A., and R. H. Johnson, 1991: Heat and moisture budgets of an intense midlatitude squall line. *J. Atmos. Sci.*, **48**, 122–146, https://doi.org/10.1175/1520-0469(1991)048<0122:HAMBOA>2.0.CO;2.

Gray, W. M., and R. W. Jacobson, 1977: Diurnal variation of deep cumulus convection. *Mon. Wea. Rev.*, **105**, 1171–1188, https://doi.org/10.1175/1520-0493(1977)105<1171:DVODCC>2.0.CO;2.

Haertel, P. T., and R. H. Johnson, 1998: Two-day disturbances in the equatorial western Pacific. *Quart. J. Roy. Meteor. Soc.*, **124**, 615–636, https://doi.org/10.1002/qj.49712454611.

——, and G. N. Kiladis, 2004: Dynamics of 2-day equatorial waves. *J. Atmos. Sci.*, **61**, 2707–2721, https://doi.org/10.1175/JAS3352.1.

Hendon, H. H., and B. Liebmann, 1994: Organization of convection within the Madden-Julian oscillation. *J. Geophys. Res.*, **99**, 8073–8083, https://doi.org/10.1029/94JD00045.

Houze, R. A., 1989: Observed structure of mesoscale convective systems and implications for large-scale heating. *Quart. J. Roy. Meteor. Soc.*, **115**, 425–461, https://doi.org/10.1002/qj.49711548702.

——, 1997: Stratiform precipitation in regions of convection: A meteorological paradox? *Bull. Amer. Meteor. Soc.*, **78**, 2179–2196, https://doi.org/10.1175/1520-0477(1997)078<2179:SPIROC>2.0.CO;2.

——, S. S. Chen, D. E. Kingsmill, Y. Serra, and S. E. Yuter, 2000: Convection over the Pacific warm pool in relation to the atmospheric Kelvin–Rossby wave. *J. Atmos. Sci.*, **57**, 3058–3089, https://doi.org/10.1175/1520-0469(2000)057<3058:COTPWP>2.0.CO;2.

Johnson, R. H., 1984: Partitioning tropical heat and moisture budgets into cumulus and mesoscale components: Implications for cumulus parameterization. *Mon. Wea. Rev.*, **112**, 1590–1601, https://doi.org/10.1175/1520-0493(1984)112<1590:PTHAMB>2.0.CO;2.

——, and P. E. Ciesielski, 2013: Structure and properties of Madden–Julian oscillations deduced from DYNAMO sounding arrays. *J. Atmos. Sci.*, **70**, 3157–3179, https://doi.org/10.1175/JAS-D-13-065.1.

——, and ——, 2017: Multiscale variability of the atmospheric boundary layer during DYNAMO. *J. Atmos. Sci.*, **74**, 4003–4021, https://doi.org/10.1175/JAS-D-17-0182.1.

——, W. A. Gallus, and M. D. Vescio, 1990: Near-tropopause vertical motion within the trailing stratiform region of a midlatitude squall line. *J. Atmos. Sci.*, **47**, 2200–2210, https://doi.org/10.1175/1520-0469(1990)047<2200:NTVMWT>2.0.CO;2.

——, P. E. Ciesielski, and K. A. Hart, 1996: Tropical inversions near the 0°C level. *J. Atmos. Sci.*, **53**, 1838–1855, https://doi.org/10.1175/1520-0469(1996)053<1838:TINTL>2.0.CO;2.

——, T. M. Rickenbach, S. A. Rutledge, P. E. Ciesielski, and W. H. Schubert, 1999: Trimodal characteristics of tropical convection. *J. Climate*, **12**, 2397–2418, https://doi.org/10.1175/1520-0442(1999)012<2397:TCOTC>2.0.CO;2.

——, P. E. Ciesielski, J. H. Ruppert, and M. Katsumata, 2015: Sounding-based thermodynamic budgets for DYNAMO. *J. Atmos. Sci.*, **72**, 598–622, https://doi.org/10.1175/JAS-D-14-0202.1.

Kikuchi, K., and Y. N. Takayabu, 2004: The development of organized convection associated with the MJO during TOGA COARE IOP: Trimodal characteristics. *Geophys. Res. Lett.*, **31**, L10101, https://doi.org/10.1029/2004GL019601.

Kiladis, G. N., M. C. Wheeler, P. T. Haertel, K. H. Straub, and P. E. Roundy, 2009: Convectively coupled equatorial waves. *Rev. Geophys.*, **47**, RG2003, https://doi.org/10.1029/2008RG000266.

Kubota, H., K. Yoneyama, J.-I. Hamada, P. Wu, A. Sudaryanto, and I. B. Wahyono, 2015: Role of Maritime Continent convection during the preconditioning stage of the Madden–Julian oscillation observed in CINDY2011/DYNAMO. *J. Meteor. Soc. Japan.*, **93A**, 101–114, https://doi.org/10.2151/jmsj.2015-050.

Lau, K. M., T. Nakazawa, and C. H. Sui, 1991: Observations of cloud cluster hierarchies over the tropical western Pacific. *J. Geophys. Res.*, **96**, 3197–3208, https://doi.org/10.1029/90JD01830.

Liu, F., and B. Wang, 2012: A model for the interaction between 2-day waves and moist Kelvin waves. *J. Atmos. Sci.*, **69**, 611–625, https://doi.org/10.1175/JAS-D-11-0116.1.

Mapes, B., S. Tulich, J. Lin, and P. Zuidema, 2006: The mesoscale convection life cycle: Building block or prototype for large-scale tropical waves? *Dyn. Atmos. Oceans*, **42**, 3–29, https://doi.org/10.1016/j.dynatmoce.2006.03.003.

Mather, J. H., S. A. McFarlane, M. A. Miller, and K. L. Johnson, 2007: Cloud properties and associated radiative heating rates in the tropical western Pacific. *J. Geophys. Res.*, **112**, D05201, https://doi.org/10.1029/2006JD007555.

Nakazawa, T., 1988: Tropical super clusters within intraseasonal variations over the western Pacific. *J. Meteor. Soc. Japan.*, **66**, 823–839, https://doi.org/10.2151/jmsj1965.66.6_823.

——, 1995: Intraseasonal oscillations during the TOGA-COARE IOP. *J. Meteor. Soc. Japan.*, **73**, 305–319, https://doi.org/10.2151/jmsj1965.73.2B_305.

Randall, D. A., Harshvardhan, and D. A. Dazlich, 1991: Diurnal variability of the hydrologic cycle in a general circulation model. *J. Atmos. Sci.*, **48**, 40–62, https://doi.org/10.1175/1520-0469(1991)048<0040:DVOTHC>2.0.CO;2.

Sarachik, E. S., 1985: A simple theory for the vertical structure of the tropical atmosphere. *Pure Appl. Geophys.*, **123**, 261–271, https://doi.org/10.1007/BF00877022.

Schubert, W. H., P. E. Ciesielski, C. Lu, and R. H. Johnson, 1995: Dynamical adjustment of the trade wind inversion layer. *J. Atmos. Sci.*, **52**, 2941–2952, https://doi.org/10.1175/1520-0469(1995)052<2941:DAOTTW>2.0.CO;2.

Takayabu, Y. N., 1994a: Large-scale cloud disturbances associated with equatorial waves. Part I: Spectral features of the cloud disturbances. *J. Meteor. Soc. Japan.*, **72**, 433–449, https://doi.org/10.2151/jmsj1965.72.3_433.

——, 1994b: Large-scale cloud disturbances associated with equatorial waves. Part II: Westward-propagating inertio-gravity waves. *J. Meteor. Soc. Japan.*, **72**, 451–465, https://doi.org/10.2151/jmsj1965.72.3_451.

——, K. Lau, and C. Sui, 1996: Observation of a quasi-2-day wave during TOGA COARE. *Mon. Wea. Rev.*, **124**, 1892–1913, https://doi.org/10.1175/1520-0493(1996)124<1892:OOAQDW>2.0.CO;2.

Thomson, R. E., and W. J. Emery, 2014: *Data Analysis Methods in Physical Oceanography*. 3rd ed. Elsevier, 728 pp.

TRMM, 2011: TRMM (TMPA) rainfall estimate L3 3 hour 0.25 degree × 0.25 degree V7. Goddard Earth Sciences Data and Information Services Center, accessed 16 September 2014, https://disc.gsfc.nasa.gov/datacollection/TRMM_3B42_7.html.

UCAR/NCAR, 2012: Meteosat-7 IR (Channel 8) calibrated data in NetCDF format, version 1.0. UCAR/NCAR Earth Observing Laboratory, accessed 22 October 2014. http://data.eol.ucar.edu/dataset/347.027.

Uyeda, H., and Coauthors, 1995: Doppler radar observations on the structure and characteristics of tropical clouds during the TOGA-COARE IOP in Manus, Papua New Guinea. *J. Meteor. Soc. Japan.*, **73**, 415–426, https://doi.org/10.2151/jmsj1965.73.2B_415.

Webster, P. J., and G. L. Stephens, 1980: Tropical upper-tropospheric extended clouds: Inferences from winter MONEX. *J. Atmos. Sci.*, **37**, 1521–1541, https://doi.org/10.1175/1520-0469-37.7.1521.

Wheeler, M., and G. N. Kiladis, 1999: Convectively coupled equatorial waves: Analysis of clouds and temperature in the wavenumber–frequency domain. *J. Atmos. Sci.*, **56**, 374–399, https://doi.org/10.1175/1520-0469(1999)056<0374:CCEWAO>2.0.CO;2.

——, ——, and P. J. Webster, 2000: Large-scale dynamical fields associated with convectively coupled equatorial waves. *J. Atmos. Sci.*, **57**, 613–640, https://doi.org/10.1175/1520-0469(2000)057<0613:LSDFAW>2.0.CO;2.

Xie, S., R. T. Cederwall, and M. Zhang, 2004: Developing long-term single-column model/cloud system–resolving model forcing data using numerical weather prediction products constrained by surface and top of the atmosphere observations. *J. Geophys. Res.*, **109**, D01104, https://doi.org/10.1029/2003JD004045.

Xu, W., and S. A. Rutledge, 2014: Convective characteristics of the Madden–Julian oscillation over the central Indian Ocean observed by shipborne radar during DYNAMO. *J. Atmos. Sci.*, **71**, 2859–2877, https://doi.org/10.1175/JAS-D-13-0372.1.

Yamada, H., K. Yoneyama, M. Katsumata, and R. Shirooka, 2010: Observations of a super cloud cluster accompanied by synoptic-scale eastward-propagating precipitating systems over the Indian Ocean. *J. Atmos. Sci.*, **67**, 1456–1473, https://doi.org/10.1175/2009JAS3151.1.

Yanai, M., S. Esbensen, and J. Chu, 1973: Determination of bulk properties of tropical cloud clusters from large-scale heat and moisture budgets. *J. Atmos. Sci.*, **30**, 611–627, https://doi.org/10.1175/1520-0469(1973)030<0611:DOBPOT>2.0.CO;2.

Yanase, A., K. Yasunaga, and H. Masunaga, 2017: Relationship between the direction of diurnal rainfall migration and the ambient wind over the Southern Sumatra Island. *Earth Space Sci.*, **4**, 117–127, https://doi.org/10.1002/2016EA000181.

Yoneyama, K., and Coauthors, 2008: Mismo field experiment in the equatorial Indian Ocean. *Bull. Amer. Meteor. Soc.*, **89**, 1889–1903, https://doi.org/10.1175/2008BAMS2519.1.

——, C. Zhang, and C. N. Long, 2013: Tracking pulses of the Madden–Julian oscillation. *Bull. Amer. Meteor. Soc.*, **94**, 1871–1891, https://doi.org/10.1175/BAMS-D-12-00157.1.

Zhang, C., and K. Yoneyama, 2017: CINDY/DYNAMO field campaign: Advancing our understanding of MJO initiation. *The Global Monsoon System: Research and Forecast*, 3rd ed. C.-P. Change et al., Eds., World Scientific Series on Asia-Pacific Weather and Climate, Vol. 9, 339–348, https://doi.org/10.1142/9789813200913_0027.

Zhang, M. H., and J. L. Lin, 1997: Constrained variational analysis of sounding data based on column-integrated budgets of mass, heat, moisture, and momentum: Approach and application to ARM measurements. *J. Atmos. Sci.*, **54**, 1503–1524, https://doi.org/10.1175/1520-0469(1997)054<1503:CVAOSD>2.0.CO;2.

——, ——, R. T. Cederwall, J. J. Yio, and S. C. Xie, 2001: Objective analysis of ARM IOP data: Method and sensitivity. *Mon. Wea. Rev.*, **129**, 295–311, https://doi.org/10.1175/1520-0493(2001)129<0295:OAOAID>2.0.CO;2.

Zipser, E. J., 1977: Mesoscale and convective–scale downdrafts as distinct components of squall-line structure. *Mon. Wea. Rev.*, **105**, 1568–1589, https://doi.org/10.1175/1520-0493(1977)105<1568:MACDAD>2.0.CO;2.

Zuluaga, M. D., and R. A. Houze, 2013: Evolution of the population of precipitating convective systems over the equatorial Indian Ocean in active phases of the Madden–Julian oscillation. *J. Atmos. Sci.*, **70**, 2713–2725, https://doi.org/10.1175/JAS-D-12-0311.1.